




Local and Global Dynamics of a Ratio-Dependent Holling–Tanner Predator–Prey Model with Strong Allee Effect

Weiping Lou

*School of Mathematics and Statistics, Henan University,
Kaifeng 475001, P. R. China*

Pei Yu ^{*}

*Department of Mathematics, Western University,
London, ON, Canada N6A 5B7
pyu@uwo.ca*

Jia-Fang Zhang 

*School of Mathematics and Statistics, Henan University,
Kaifeng 475001, P. R. China*

Claudio Arancibia-Ibarra 

*Safe Food Production Queensland, Australia Faculty of Engineering
and Business, Universidad de las Americas, Providencia, Chile
carancibia-ibarra@safefood.qld.gov.au*

Received March 24, 2024; Accepted April 2, 2024; Published June 7, 2024

In this paper, the impact of the strong Allee effect and ratio-dependent Holling–Tanner functional response on the dynamical behaviors of a predator–prey system is investigated. First, the positivity and boundedness of solutions of the system are proved. Then, stability and bifurcation analysis on equilibria is provided, with explicit conditions obtained for Hopf bifurcation. Moreover, global dynamics of the system is discussed. In particular, the degenerate singular point at the origin is proved to be globally asymptotically stable under various conditions. Further, a detailed bifurcation analysis is presented to show that the system undergoes a codimension-1 Hopf bifurcation and a codimension-2 cusp Bogdanov–Takens bifurcation. Simulations are given to illustrate the theoretical predictions. The results obtained in this paper indicate that the strong Allee effect and proportional dependence coefficient have significant impact on the fundamental change of predator–prey dynamics and the species persistence.

Keywords: Strong Allee effect; Hopf bifurcation; saddle-node bifurcation; Bogdanov–Takens bifurcation; global dynamics.

1. Introduction

There are many interaction forms between species in the ecological environment, such as competition, predation, cooperation and so on. Predator–prey interaction, which is regarded as the most important basic interspecies relations whenever in

ecological or social respects, has been explored for many years. [Lotka](#) [\[1925\]](#) and [Volterra](#) [\[1926\]](#) constructed the predator–prey differential equation model (called Lotka–Volterra equation) in 1920s, which was the first attempt for people to discover ecological laws. After their pioneering work, the

*Author for correspondence

traditional predator–prey models attracted the interest of many researchers [Berryman, 1992; Bazykin, 1998; Freedman, 1980; Huo & Li, 2004; Ruan & Xiao, 2000; Yan & Li, 2006; Zeng et al., 2020].

For the most predator–prey models, the prey is usually assumed to grow with a Logistic pattern. However, in 1930s, [Allee and Aggregations, 1931] posed a critical question: Does there exist a minimal number for a species, which guarantees its survival in nature? Allee discussed the significant impact of crowding on demography and life disposition, and found that the growth rate of small density is not always positive, nor can it decrease as much as the Logistic model. Therefore, species may have the growth rate of Allee effect due to mate restriction, cooperative feeding between species, dispersion of species in space and habitat change [Arancibia-Ibarra & Flores, 2021; Sen et al., 2022]. Mathematically, the most common continuous growth equation with the Allee effect takes the form:

$$\frac{dx}{dt} = r \left(1 - \frac{x}{K} \right) (x - A)x,$$

where $x = x(t)$ represents the prey size for $t \geq 0$, and A measures the Allee effect. The so-called strong Allee effect and weak Allee effect are defined by the positive ($A > 0$) or the negative ($A < 0$) critical threshold, respectively [Sen et al., 2022; Wang et al., 2011; Wang & Kot, 2002]. A strong Allee effect implies that the per capita growth rate is negative in the limit of a low density; while if the per capita growth is positive when it has a zero density, then it is called weak Allee effect. The Allee effect can emerge at the population level due to a variety of mechanisms including enhancement in foraging efficiency, reproductive facilitation, collective defense and the modification of environmental conditions by organisms. Generally speaking, the Allee effect indicates that the prey population has a positive density-dependent growth rate when it has a low density, which is recognized as the prey may have a growth rate [Boukal et al., 2007; Gascoigne & Lipcius, 2004; Lewis & Kareiva, 1993; Morozov et al., 2006]. It should be noted that the Allee effect may have different forms in different cases. For instance, the well-known depensation phenomenon in fishing models generates a negative competition effect in the case where the growth rate of the population is negative, leading to the existence of an extinction threshold [Ni & Wang, 2017; Zeng & Yu, 2022; Verma & Misra, 2018].

Among the widely used mathematical models in theoretical ecology, the Leslie–Gower prey–predator model plays a special role because of its fundamental dynamics, and it is considered as a prototypical prey–predator system [May, 1998; Pielou, 1969; Pal & Mandal, 2014]. The classical Leslie–Gower prey–predator model proposed by Leslie and studied by [Leslie & Gower, 1960] is described by the following equations:

$$\begin{cases} \dot{u} = u(1 - u) - \beta uv, \\ \dot{v} = cv \left(1 - \frac{v}{u} \right), \end{cases} \quad (1)$$

where the dot represents differentiation with respect to time t , $u = u(t)$ and $v = v(t)$ denote the population densities of the prey and the predator at time t , respectively. The positive constants β and c denote the maximum per capita consumption rate of predators and the intrinsic growth rate of the predator, respectively. It is known that system (1) has a globally asymptotically stable equilibrium [Korobeinikov, 2001] and many research results have been obtained [Ni & Wang, 2017; Song et al., 2009].

The predatory functional response is often used to describe the transfer of nutrient levels between prey and predator populations, and many well-known functional response functions including Holling types I, II, III [Holling, 2004] have been widely applied in research. In reality, they are functions that reflect differences in energy transfer patterns in nature or the ability of predators to capture prey. A more realistic functional response function should be not only related to the prey, but also related to the predator [Artidi & Ginzburg, 1989; Boukal et al., 2007; Hsu et al., 2001a, 2001b]. The discussion on the historical biological relevance of the classical prey-dependent model and the ratio-dependent model is available [Arino et al., 2004]. Furthermore, many authors analyzed the biological significance of the ratio-dependent response function [Kuang & Beretta, 1998], and showed that it could be derived from the Michaelis–Menten (or the Holling type II) functional response $\frac{muv}{a+x}$ [Freedman, 1980]. When $x = \frac{u}{v}$, it generates the ratio-dependent response functional in the form of $\frac{muv}{u+av}$. Moreover, they also discussed that the ratio-dependent predator–prey models exhibit rich dynamics in boundary-value problems. Modeling and analysis of predator–prey systems in each particular case should be further developed in

accordance with ratio dependence theory, which have been studied for the last 30 years [Beretta & Kuang, 1998; Lajmimi *et al.*, 2018; Maimul, 2009; Xiao & Ruan, 2018; Zhang *et al.*, 2022].

In this paper, we will consider the Leslie–Gower predator–prey model which has a ratio-dependent functional response and involves the strong Allee effect for the predator consuming the prey. The model is given as follows:

$$\begin{cases} \dot{u} = u \left[\frac{1}{b}(1-u)(u-b) - \frac{mv}{u+av} \right], \\ \dot{v} = cv \left(1 - \frac{v}{u} \right), \\ u(0) = u_0 \geq 0, \quad v(0) = v_0 \geq 0, \end{cases} \quad (2)$$

where all parameters a , b , c and m take positive values. m is the capturing rate of prey by predator. a and c , respectively, represent the saturation rate of the predator and a measure of the growth rate of the predator. The parameter b is restricted to $b \in (0, 1)$, representing the Allee threshold value: A strong Allee effect introduces a population threshold, and the population must surpass this threshold to grow.

The role of the strong Allee effect in population dynamics has been largely addressed in the theoretical literature. In this paper, we will consider the dynamics of system (2). In order to simplify the analysis of system, a feedback control law is obtained which stabilizes the closed loop system [Arancibia-Ibarra *et al.*, 2019; Arancibia-Ibarra & Flores, 2021]. Since system (2) includes the ratio-dependent functional responses $\frac{mv}{u+av}$ and $\frac{v}{u}$, it is challenging to study the local topological structure near the origin since it is a degenerate singular point and usually the blow-up approach is applied. We will establish the positivity and boundedness of the solutions of system (2), and give a detailed study on the stability and bifurcation of equilibrium solutions. There exist a trivial equilibrium at the origin, two boundary equilibria and one or two positive (interior) equilibria. In particular, the degenerate singular point at the origin is proved to be globally asymptotically stable under various conditions. Moreover, we will show that both Hopf and Bogdanov–Takens (BT) bifurcations can occur from the positive equilibrium, and prove that the codimension of the Hopf bifurcation is one, implying that there does not exist generalized Hopf bifurcation. The codimension of the BT bifurcation is

shown as two and detailed bifurcation curves on the saddle-node, Hopf and homoclinic loop bifurcations are given. Numerical simulations are presented to illustrate the theoretical results, including the global trapping region, typical bifurcation diagrams, showing the global dynamical behaviors of system (2).

The rest of the paper is organized as follows. In Sec. 2 the positivity and boundedness of the solutions of system (2) are established. In Sec. 3 we give analysis on the stability and bifurcation of equilibria. Section 4 is devoted to consider the topological structure of the origin and derive the conditions under which $(0, 0)$ is globally asymptotically stable, and discuss the dynamical properties of the solutions of system (2). In Sec. 5 we further study saddle-node, Hopf and BT bifurcations, and pay attention to their codimensions. Simulations are present in Sec. 6, and the conclusion is drawn in Sec. 7.

2. Positivity and Boundedness of Solutions

The solutions of a biological system are usually positive and bounded. Thus, in this section, we prove the following theorem for the positivity and boundedness of the solutions of system (2).

Theorem 1. *The solutions of system (2) are positive provided the initial conditions are positive, and they are bounded.*

Proof. It is easy to show that the solutions of system (2) are positive provided that the initial conditions are positive. By variation of parameters, we can write the solutions of system (2) as

$$\begin{aligned} u(t) &= u(0)e^{\int_0^t \left[\frac{1}{b}(1-u(s))(u(s)-b) - \frac{mv(s)}{u(s)+av(s)} \right] ds}, \quad t > 0 \\ v(t) &= v(0)ce^{\int_0^t \left[1 - \frac{v(s)}{u(s)} \right] ds}, \quad t > 0, \end{aligned}$$

which clearly indicates that for $t > 0$, $u(t) > 0$ if $u(0) > 0$ and $v(t) > 0$ if $v(0) > 0$.

Proving the boundedness of the solutions is not straightforward. First, note that the u -axis ($v = 0$) is invariant, and that $\frac{du}{dt} \rightarrow 0^+$ and $\frac{dv}{dt} \rightarrow -\infty$ as $u \rightarrow 0^+$. This implies that trajectories of system (2) cannot cross the u -axis and v -axis. Thus, we construct a triangle trapping region, bounded by the u -axis, v -axis and the line:

$$\mathcal{L} : u + \frac{4am}{c(a+1)^2}v = k,$$

where the positive constant k is to be determined. Let

$$Q(u, v) = u + \frac{4am}{c(a+1)^2}v,$$

which is positive definite and radially unbounded, with $Q(0,0) = 0$. Then, differentiating Q with respect to time t and evaluating it along the trajectory of system (2), we obtain

$$\begin{aligned} \left. \frac{dQ}{dt} \right|_{(2)} &= \frac{du}{dt} + \frac{4am}{c(a+1)^2} \frac{dv}{dt} \\ &= \frac{u}{b}(1-u)(u-b) - \frac{muv}{u+av} \\ &\quad + \frac{4am}{(a+1)^2}v \left(1 - \frac{v}{u}\right) \\ &= \frac{u}{b}(1-u)(u-b) - \frac{4a^2mv}{(a+1)^2u(u+av)} \\ &\quad \times \left(v - \frac{a-1}{2a}u\right)^2. \end{aligned}$$

It is obvious that $\left. \frac{dQ}{dt} \right|_{(2)} < 0$ for $u \in (0, b] \cup [1, \infty)$ and $v \in (0, \infty)$. Thus, we only need to consider $u \in (b, 1)$ for two cases: $a \leq 1$ and $a > 1$.

When $a \leq 1$, we have $u(u+av) < 1+v$ and $v + \frac{1-a}{2a}u \geq v$. Moreover, it is easy to show that the term $\frac{u}{b}(1-u)(u-b)$ has its maximal value,

$$\begin{aligned} \alpha_1 &= \frac{(1+b)(2-b)(1-2b) + 2(1-b+b^2)^{\frac{3}{2}}}{27b} \\ &> 0, \end{aligned} \tag{3}$$

for $0 < b < 1$. Hence, we obtain $\left. \frac{dQ}{dt} \right|_{(2)} < \alpha_1 - \frac{a^2mv^3}{1+v}$, for which there exists $\tilde{v}_1 > 0$ such that

$$\begin{aligned} \left. \frac{dQ}{dt} \right|_{(2)} &< \alpha_1 - \frac{a^2mv^3}{v+1} \\ &= -\frac{a^2m}{v+1} \left[v^3 - \frac{\alpha_1}{a^2m}(v+1) \right] \\ &< 0 \end{aligned}$$

for $v > \tilde{v}_1$. To determine \tilde{v}_1 , we use the equation:

$$\begin{aligned} \tilde{v}_1^3 - \frac{\alpha_1}{a^2m}(\tilde{v}_1 + 1) &> \tilde{v}_1^3 - \tilde{v}_1 - \frac{\alpha_1}{a^2m}(\tilde{v}_1 + 1) \\ &= (\tilde{v}_1 + 1) \left(\tilde{v}_1^2 - \tilde{v}_1 - \frac{\alpha_1}{a^2m} \right) \\ &\geq 0, \end{aligned}$$

which yields

$$\tilde{v}_1 \geq \frac{1}{2} \left(1 + \sqrt{1 + \frac{4\alpha_1}{a^2m}} \right),$$

and thus \tilde{v}_1 can be taken as

$$\tilde{v}_1 = \frac{1}{2} \left(1 + \sqrt{1 + \frac{4\alpha_1}{a^2m}} \right). \tag{4}$$

Therefore, for $a \leq 1$, we choose k for the line \mathcal{L} as

$$\begin{aligned} k_1 &= 1 + \frac{4am}{c(a+1)^2}\tilde{v}_1 \\ &= 1 + \frac{2am}{c(a+1)^2} \left(1 + \sqrt{1 + \frac{4\alpha_1}{a^2m}} \right). \end{aligned} \tag{5}$$

Next, consider $a > 1$. We take $v > \frac{a-1}{2a}u$, and obtain $\frac{v}{u+av} > \frac{a-1}{a(a+1)}$. Then,

$$\begin{aligned} \left. \frac{dQ}{dt} \right|_{(2)} &< \frac{u}{b}(1-u)(u-b) \\ &\quad - \frac{4a(a-1)m}{(a+1)^3u} \left(v - \frac{a-1}{2a}u \right)^2 \\ &= \frac{1}{u} \left[\frac{u^2}{b}(1-u)(u-b) \right. \\ &\quad \left. - \frac{4a(a-1)m}{(a+1)^3} \left(v - \frac{a-1}{2a}u \right)^2 \right] \\ &< \frac{1}{u} \left[\alpha_2 - \frac{4a(a-1)m}{(a+1)^3} \left(v - \frac{a-1}{2a}u \right)^2 \right], \end{aligned}$$

where α_2 is the maximal value of $\frac{u^2}{b}(1-u)(u-b)$ in $b < u < 1$, given by

$$\alpha_2 = \frac{27(1+b^4) - 36b(1+b^2) + 2b^2 + (1+b)(9-14b+9b^2)^{\frac{3}{2}}}{512b} > 0 \tag{6}$$

for $0 < b < 1$. This again shows that there exists $\tilde{v}_2 > 0$ such that

$$\left. \frac{dQ}{dt} \right|_{(2)} < \frac{1}{u} \left[\alpha_2 - \frac{4a(a-1)m}{(a+1)^3} \left(v - \frac{a-1}{2a}u \right)^2 \right] \leq 0$$

for $v > \tilde{v}_2$. To determine \tilde{v}_2 , we use the equation:

$$\begin{aligned} \left(\tilde{v}_2 - \frac{a-1}{2a}u\right)^2 &\geq \frac{(a+1)^3\alpha_2}{4a(a-1)m} \Rightarrow \tilde{v}_2 \\ &\geq \frac{a-1}{2a}u + \frac{a+1}{2}\sqrt{\frac{(a+1)\alpha_2}{a(a-1)m}}, \end{aligned}$$

and thus we can take

$$\tilde{v}_2 = \frac{a-1}{2a} + \frac{a+1}{2}\sqrt{\frac{(a+1)\alpha_2}{a(a-1)m}}. \tag{7}$$

Hence, for $a > 1$, we choose k for the line \mathcal{L} as

$$\begin{aligned} k_2 &= 1 + \frac{4am}{c(a+1)^2}\tilde{v}_2 \\ &= 1 + \frac{2am}{c(a+1)^2}\left(\frac{a-1}{a} + (a+1)\sqrt{\frac{(a+1)\alpha_2}{a(a-1)m}}\right). \end{aligned} \tag{8}$$

Now, we use (5) and (8) to take $k = \max\{k_1, k_2\}$, and then construct the trapping region, defined by

$$\Omega_0 = \left\{ (u, v) \mid u \geq 0, v \geq 0, u + \frac{4am}{c(a+1)^2}v \leq k \right\}, \tag{9}$$

which attracts all trajectories starting from any initial points in the first quadrant of the u - v plane. The trapping area is shown in Fig. 1

This finishes the proof for Theorem 1 ■

Thus, in the following analysis, we only need to consider the solutions restricted to Ω_0 . Note that

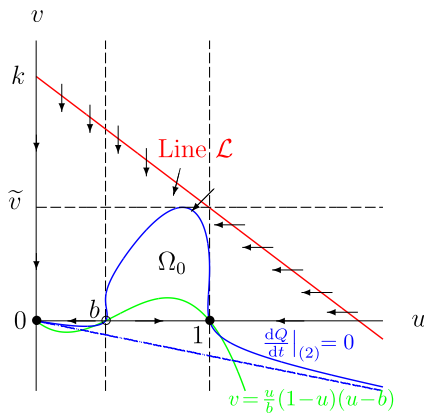


Fig. 1. The trapping region Ω_0 for system (2), bounded by the u -axis, v -axis and the straight line \mathcal{L} in the first quadrant of the u - v plane, where $\tilde{v} = \tilde{v}_1$ for $0 < a \leq 1$ and $\tilde{v} = \tilde{v}_2$ for $a > 1$.

the triangle trapping region Ω_0 may be reduced to the Trapezoidal region $\tilde{\Omega}_0$, defined by

$$\tilde{\Omega}_0 = \left\{ (u, v) \mid 0 \leq u \leq 1, v \geq 0, u + \frac{4am}{c(a+1)^2}v \leq k \right\}. \tag{10}$$

3. Stability and Bifurcation of Equilibria

In this section, we focus on investigating the existence and stability conditions of the equilibria of system (2). To achieve this, letting the right-hand side of system (2) equal zero, we have

$$\begin{aligned} \frac{u}{b}(1-u)(u-b) - \frac{muv}{u+av} &= 0 \quad \text{and} \\ cv\left(1 - \frac{v}{u}\right) &= 0, \end{aligned}$$

which yields the following equilibrium solutions:

$$\begin{aligned} E_0 &: (0, 0), && \text{Trivial equilibrium,} \\ E_1 &: (1, 0), && \text{Boundary equilibrium,} \\ E_2 &: (b, 0), && \text{Boundary equilibrium,} \\ E_3 &: (u_3, u_3), && \text{Positive equilibrium,} \end{aligned} \tag{11}$$

where u_3 is the positive root of the quadratic polynomial:

$$F_1(u_3) = u_3^2 - (b+1)u_3 + b\left(1 + \frac{m}{a+1}\right). \tag{12}$$

The equilibrium $(0, 0)$ is a degenerate singular point. The topological structure near this singular point is complex and will be discussed in the following section using the “blow-up” approach.

Define

$$m^* = \frac{(a+1)(1-b)^2}{4b}, \quad \Delta = 4b(a+1)(m^* - m), \tag{13}$$

and the parameter space,

$$\begin{aligned} \Gamma_4 &= \{ \gamma = (a, b, m, c) \mid \\ &a > 0, c > 0, m > 0, 0 < b < 1 \}. \end{aligned} \tag{14}$$

Then, for the existence and stability of the nonzero equilibria $E_k, k = 1, 2, 3$, we have the following theorem.

Theorem 2. For system (2), the equilibria E_1 and E_2 exist for any feasible parameter $\gamma \in \Gamma_4$, while

the equilibrium E_3 exists for $\gamma \in \Gamma_4$ and if

$$\begin{cases} m = m^* : u_3 = \frac{1}{2}(1+b), \\ \text{yielding one equilibrium: } E_3 = (u_3, u_3) \text{ or} \\ m < m^* : u_{3\pm} = \frac{1}{2} \left(1 + b \pm \frac{\sqrt{\Delta}}{a+1} \right), \\ \text{yielding two equilibria: } E_{3\pm} = (u_{3\pm}, u_{3\pm}), \end{cases} \quad (15)$$

satisfying $b < E_3$, $E_{3\pm} < 1$. E_1 is a saddle and E_2 is an unstable node for any $\gamma \in \Gamma_4$. When $m < m^*$, E_3 does not exist. When $m = m^*$, E_3 is a degenerate stable (unstable) node if $c > c_u$ ($c < c_u$). When $m < m^*$, E_{3-} is a saddle point, while E_{3+} is Locally Asymptotically Stable (LAS) if one of the following three conditions holds: (i) $c \geq c_u$, (ii) $c < c_u$ when $m \leq m_*$, (iii) $c < \min\{1-b, c_u\}$ or $c \in [1-b, c_u]$ with $b < \frac{1}{4a+5}$ when $m_* < m < m_H (< m^*)$, and is unstable for $m_H < m < m^*$. Hopf bifurcation occurs from E_{3+} at the critical point $m = m_H$. Here,

$$c_u = \frac{(1-b)^2}{4b(a+1)} = \frac{m^*}{(a+1)^2},$$

$$\begin{aligned} m_* &= \frac{[(1-b)^2 + 2bc](a+1)^2}{2b(2a+3)}, \\ m_H &= \frac{1}{2b(2a+3)^2} \{ (a+1)^2[(a+2)(1-b)^2 \\ &\quad - 4b(a+1) + 2bc(2a+3)] + \sqrt{\Delta_1} \}, \\ \Delta_1 &= (a+1)^4(1+b)^2[a^2(1+b)^2 + 4a(1+b)^2 \\ &\quad + 4(1-b+b^2) - 4bc(2a^2 + 5a + 3)]. \end{aligned} \quad (16)$$

Proof. The existence conditions for the equilibria E_1 and E_2 are obvious. For the equilibrium E_3 , it suffices to consider the real positive solutions of $F_1 = 0$, which depends upon Δ : when $\Delta < 0$ ($m > m^*$), $F_1 = 0$ has no real roots; when $\Delta = 0$ ($m = m^*$), $F_1 = 0$ has one positive real root; and when $\Delta > 0$ ($m < m^*$), $F_1 = 0$ has two positive real roots. This gives the equilibrium E_3 and $E_{3\pm}$ in (15). It is obvious that $b < u_3 < 1$. Moreover, a direct computation shows that

$$b < u_{3-} < u_{3+} < 1 \quad \text{for } m < m^*.$$

To find the stability of equilibria, we calculate the Jacobian of system (15) to obtain

$$J(u, v) = \begin{bmatrix} -\frac{1}{b}[3u^2 - 2(1+b)u + b] - \frac{mav^2}{(u+av)^2} & -\frac{mu^2}{(u+av)^2} \\ \frac{cv^2}{u^2} & c \left(1 - \frac{2v}{u} \right) \end{bmatrix}. \quad (17)$$

Evaluating J at E_1 and E_2 yields

$$\begin{aligned} J(E_1) &= \begin{bmatrix} 1 - \frac{1}{b} & -m \\ 0 & c \end{bmatrix}, \\ J(E_2) &= \begin{bmatrix} 1 - b & -m \\ 0 & c \end{bmatrix}, \end{aligned}$$

which clearly indicates that E_1 is a saddle point and E_2 is an unstable node for any $\gamma \in \Gamma_4$.

Next, evaluating J at E_3 , which exists for $m = m^*$, gives the trace and determinant of $J(E_3)$ as

$$\text{Tr}(J(E_3)) = -(c - c_u), \quad \det(J(E_3)) = 0, \quad (18)$$

showing that E_3 is a degenerate singular point. We apply center manifold theory to further consider the stability of E_3 . We introduce the transformation,

$$\begin{pmatrix} u \\ v \end{pmatrix} = \begin{pmatrix} \frac{1}{2}(1+b) \\ \frac{1}{2}(1+b) \end{pmatrix} + \begin{bmatrix} 1 & c_u \\ 1 & c \end{bmatrix} \begin{pmatrix} x_1 \\ x_2 \end{pmatrix}, \quad (19)$$

into (2) to obtain the following system:

$$\begin{cases} \dot{x}_1 = -\frac{c(1+b)}{4b(a+1)(c-c_u)} \\ \quad \times \left[2(a+1)x_1^2 + \frac{(1-b)^2}{b}x_1x_2 + \dots \right], \\ \dot{x}_2 = -(c-c_u)x_2 + \frac{c(1+b)}{4b(a+1)(c-c_u)} \\ \quad \times \left[2(a+1)x_1^2 + \frac{(1-b)^2}{b}x_1x_2 + \dots \right]. \end{cases}$$

Assume the center manifold is expressed as $x_2 = h_2 x_1^2$. Then, using $\dot{x}_2 = 2h_2 x_1 \dot{x}_1$ together with the above equations we find h_2 , leading to the center manifold,

$$\text{CM} = \left\{ (x_1, x_2) \mid x_2 = \frac{8b(1+b)(a+1)^2}{[4b(a+1)(c-c_u)]^2} x_1^2 + O(x_1^3) \right\}, \tag{20}$$

and the differential equation describing the dynamics on the CM, given by

$$\dot{x}_1 = -\frac{2c(1+b)(a+1)}{4b(a+1)(c-c_u)} x_1^2 + O(x_1^3), \tag{21}$$

which, together with (18), clearly shows that E_3 is a degenerate stable (unstable) node for $c > c_u$ ($c < c_u$). When $m = m^*$ and $c = c_u$, the system undergoes BT bifurcation, which will be discussed later in Sec. 5.3.

Now, consider the stability of E_{3-} and E_{3+} which exist for $m < m^*$. Evaluating J at E_{3-} , we obtain the determinant

$$\begin{aligned} \det(J(E_{3-})) &= -\frac{2c}{(a+1)(a+1+m) \left[1 + \frac{(1+b)\sqrt{a+1}}{\sqrt{4b(m^*-m)}} \right]} < 0, \end{aligned}$$

implying that E_{3-} is a saddle. Similarly, evaluating the Jacobian at E_{3+} we have

$$\begin{aligned} \det(J(E_{3+})) &= \frac{c\sqrt{m^*-m}}{\sqrt{b(a+1)}} \left[1 + b + \sqrt{\frac{4b}{a+1}(m^*-m)} \right] > 0. \end{aligned}$$

Hence, the stability of the equilibrium E_{3+} is determined by the trace of $J(E_{3+})$, which is given by

$$\begin{aligned} \text{Tr}(J(E_{3+})) &= -\frac{1}{2b} \left[(1-b)^2 + 2bc - \frac{2bm(2a+3)}{(a+1)^2} \right. \\ &\quad \left. + (b+1)\sqrt{\frac{4b}{a+1}(m^*-m)} \right]. \end{aligned}$$

In the following, we derive the stability of E_{3+} and the condition for Hopf bifurcation from E_{3+} ,

expressed in terms of the system parameters. First, it is easy to see that $\text{Tr}(J(E_{3+})) < 0$ for

$$(1-b)^2 + 2bc - \frac{2bm(2a+3)}{(a+1)^2} \geq 0,$$

which is combined with $m < m^*$ to yield

$$c < c_u, \quad m \leq m_* \quad \text{or} \quad c \geq c_u, \quad m < m^*, \tag{22}$$

under which E_{3+} is asymptotically stable, where c_u , m_* and m^* are given in (15) and (16), respectively.

On the other hand, when

$$(1-b)^2 + 2bc - \frac{2bm(2a+3)}{(a+1)^2} < 0,$$

we have

$$m_* < m < m^*, \quad \text{which requires } c < c_u.$$

Then,

$$\begin{aligned} \text{Tr}(J(E_{3+})) &\geq 0 \\ \Leftrightarrow (b+1)\sqrt{(1-b)^2 - \frac{4bm}{a+1}} + (1-b)^2 \\ &\quad + 2bc - \frac{2bm(2a+3)}{(a+1)^2} \leq 0, \end{aligned}$$

which is equivalent to $\tilde{G}_1 = -\frac{4b}{(a+1)^2} G_1 \leq 0$, where

$$\begin{aligned} G_1 &= b(2a+3)^2 m^2 - (a+1)^2 [(a+2)(1-b)^2 \\ &\quad - 4b(a+1) + 2bc(2a+3)]m \\ &\quad + (c+b-1)(1-b+bc)(a+1)^4. \end{aligned} \tag{23}$$

Thus,

$$\text{Tr}(J(E_{3+})) \geq 0 \Leftrightarrow G_1 \geq 0.$$

The discriminant of G_1 equals Δ_1 given in (16). A direct computation shows that

$$\Delta_1 > \Delta_1|_{c=c_u} = (a+1)^6 (b+1)^4 > 0,$$

implying that G_1 always has two real roots, denoted by

$$\begin{aligned} m_{\pm} &= \frac{1}{2b(2a+3)^2} \left\{ (a+1)^2 [(a+2)(1-b)^2 \right. \\ &\quad \left. - 4b(a+1) + 2bc(2a+3)] \pm \sqrt{\Delta_1} \right\}. \end{aligned}$$

We consider two cases for G_1 : (i) $c+b-1 < 0$ yielding $c < \min\{1-b, c_u\}$, and (ii) $c+b-1 \geq 0$, giving $c \in [1-b, c_u]$, which requires $b < \frac{1}{4a+5}$. For the case (i), $m_- < 0 < m_+$. Further, it can be shown that

$$G_1|_{m=m_*} < 0, \quad G_1|_{m=m^*} > 0,$$

implying that $m_* < m_+ < m^*$, since G_1 is a quadratic polynomial in m , leading to a graph of parabola open in the upwards direction. Hence, for the case (i), we have

$$E_{3+} \begin{cases} \text{LAS} & \text{for } c < \min\{1-b, c_u\}, \\ & m_* < m < m_H, \\ \text{unstable} & \text{for } c < \min\{1-b, c_u\}, \\ & m_H < m < m^*, \end{cases} \quad (24)$$

where

$$m_H = m_+.$$

Next, consider the case (ii). We first show that under the conditions $c \in [1-b, c_u)$ and $b < \frac{1}{4a+5}$,

the following holds:

$$\begin{aligned} & (a+2)(1-b)^2 - 4b(a+1) + 2bc(2a+3) \\ & > (a+2)(1-b)^2 - 4b(a+1) \\ & \quad + 2b(1-b)(2a+3) \\ & = \frac{1+b}{2b(2a+3)} [a+2 - (3a+4)b] \\ & > \frac{4}{(4a+5)^2} (a+1)(2a+3)^2 \\ & > 0, \end{aligned}$$

indicating that G_1 has two positive roots: $0 < m_- < m_H$. It has been shown in the above that $m_* < m_H < m^*$. Further, a direct calculation shows

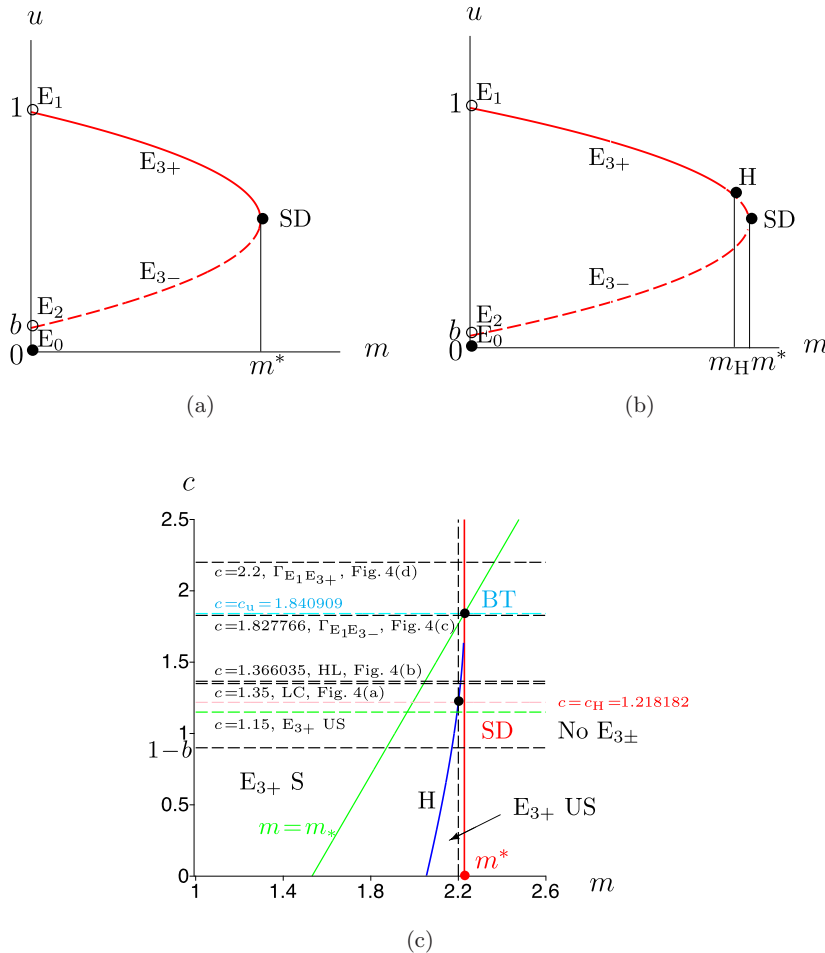


Fig. 2. Bifurcation diagrams: (a) with one perturbation parameter projected on the m - u plane without Hopf bifurcation; (b) with one perturbation parameter projected on the m - u plane with Hopf bifurcation; and (c) with two perturbation parameters plotted on the m - c plane with fixed $a = b = 0.1$. The solid and dashed curves in (a) and (b) denote, respectively, the stable and unstable equilibria. SD, H, BT, S, US, LC and HL represent the saddle-node bifurcation, Hopf bifurcation, BT bifurcations, stable, unstable, limit cycle and homoclinic loop, respectively.

that $m_- < m_*$. Therefore, we have the results for the case (ii):

$$E_{3+} \begin{cases} \text{LAS} & \text{for } b < \frac{1}{4a+5}, \quad c \in [1-b, c_u), \\ & m_* < m < m_H, \\ \text{unstable} & \text{for } b < \frac{1}{4a+5}, \quad c \in [1-b, c_u), \\ & m_H < m < m^*. \end{cases} \quad (25)$$

Summarizing the above results proves Theorem 2. ■

Using Theorem 2 typical bifurcation diagrams with one perturbation parameter m are obtained, as shown in Figs. 2(a) and 2(b), one without Hopf bifurcation [Fig. 2(a)] and one with Hopf bifurcation [Fig. 2(b)]. These two bifurcation diagrams clearly indicate the relation between the equilibrium solutions and the bifurcation parameter m . It is certainly possible to have more parameters involved in bifurcation diagram. Such a bifurcation diagram, as the one given in Fig. 2(c) using m and c as two bifurcation parameters (with fixed $a = b = 0.1$ to match the numerical bifurcation diagram shown in Fig. 7), can show bifurcation relation between more parameters (with more freedom), but its shortcoming is not able to directly demonstrate the relation of the perturbation parameters with the state variables. It is shown in Fig. 2(c) that the saddle-node bifurcation occurs from the red critical line ($m = m^*$), and no positive equilibria exist for $m > m^*$. Two positive equilibria $E_{3\pm}$ emerge from the saddle-node bifurcation, and E_{3-} is always a saddle, while Hopf bifurcation happens from E_{3+} at the blue critical curve ($m = m_H$). E_{3+} is asymptotically stable in the region on the left side of the blue and red curves, and unstable in the region bounded by the blue and red curves. The BT bifurcation occurs at the intersection point of the saddle-node and Hopf bifurcations, where the two positive equilibria $E_{3\pm}$ coincide into a single positive equilibrium E_3 . Note that the numerical bifurcation diagram given in Fig. 7, obtained by using MATCONT, shows the homoclinic loop bifurcation curve, while Fig. 2(c) does not show this curve. The Hopf and BT bifurcations and their simulations will be discussed in more detail in the following two sections.

4. Global Dynamical Properties of the Solutions

In the previous section, we focused on the local dynamical behaviors of system (2) near equilibrium solutions. In this section, we will discuss some global properties on the solutions of system (2) and provide estimates for the solutions to verify the population threshold. Since the positivity and boundedness of the solutions of system (2) have been proved in Sec. 2 with the attracting region Ω_0 defined in (9), in the following, we only need to consider the solutions bounded by Ω_0 .

For convenience, we list here some notations used in Sec. 3

$$m^* = \frac{(a+1)(1-b)^2}{4b}, \quad c_u = \frac{m^*}{(a+1)^2},$$

$$\Delta = 4b(a+1)(m^* - m), \quad u_3 = v_3 = \frac{1}{2}(1+b),$$

$$u_{3\pm} = v_{3\pm} = \frac{1}{2} \left(1 + b \pm \frac{\sqrt{\Delta}}{a+1} \right).$$

First, it is noted from the reaction terms $\frac{mv}{u+av}$ and $\frac{u}{u}$ that system (2) is not well defined at the origin $(0, 0)$. However, considering the biological meanings of $(0, 0)$, it is important to discuss the dynamical behavior around the singular point $(0, 0)$. So, we redefine system (2) as

$$\begin{cases} \dot{u} = u \left[\frac{1}{b}(1-u)(u-b) - \frac{mv}{u+av} \right], \\ \dot{v} = cv \left(1 - \frac{v}{u} \right), \\ \dot{u} = \dot{v} = 0, \quad \text{when } (u, v) = (0, 0). \end{cases} \quad (26)$$

It is easy to show that system (26) is continuous and satisfies the Lipschitz condition in the closed first quadrant in the u - v -plane, denoted by $I = \{(u, v) : u \geq 0, v \geq 0\}$. However, system (26) cannot be linearized at $(0, 0)$, and thus the local stability of $(0, 0)$ cannot be studied. Since we are only interested in the dynamics of system (26) in the interior of the first quadrant, namely, in $I^+ = \{(u, v) : u > 0, v > 0\}$, with the blow-up approach we can make a time rescaling, $dt = u(u+av)d\tau$, such that system (26) is equivalent to the following system in I^+ :

$$\frac{du}{d\tau} = U_3(u, v) + \Phi(u, v), \quad \frac{dv}{d\tau} = V_3(u, v), \quad (27)$$

where U_3 and V_3 are the third-degree homogeneous polynomials in u and v , and Φ is a higher-degree polynomial, given by

$$\begin{aligned} U_3(u, v) &= -u^2[u + (a + m)v], \\ V_3(u, v) &= cv \left(1 - \frac{v}{u}\right), \\ \Phi(u, v) &= \frac{1}{b}u^3(1 + b - u)(u + av). \end{aligned} \tag{28}$$

It is easy to see that system (27) is analytic in a neighborhood of the origin. By Theorem 3.10 in [Zhang et al., 1991], we know that any orbit of (27) tending to the origin must reach it spirally or along a fixed direction, which depends on the characteristic equation of system (27). More precisely, we have the following result.

Theorem 3. All orbits of system (27) near the origin in I^+ tend to $(0, 0)$ along the direction $\theta = \theta_1$, where θ_1 is determined by

$$\begin{aligned} \tan \theta_1 &= \frac{1}{2ac} [m + a + (a - 1)c \\ &\quad + \sqrt{(m + a + (a - 1)c)^2 + 4ac(1 + c)}] \end{aligned} \tag{29}$$

for $\theta_1 \in (0, \frac{\pi}{2})$.

Proof. We introduce the polar coordinates: $u = r \cos \theta$, $v = r \sin \theta$ into system (27), and then define the characteristic equation as

$$\begin{aligned} G(\theta) &= \cos \theta V_3(\cos \theta, \sin \theta) - \sin \theta U_3(\cos \theta, \sin \theta) \\ &= \sin \theta \cos \theta \{ [1 + (a + 1)c] \cos^2 \theta \\ &\quad + [m + a + (a - 1)c] \sin \theta \cos \theta - ac \} \\ &= -\sin \theta \cos^3 \theta \{ ac \tan^2 \theta \\ &\quad - [m + a + (a - 1)c] \tan \theta - (c + 1) \}. \end{aligned} \tag{30}$$

Besides the two trivial solutions: $\theta = 0, \frac{\pi}{2}$, $G(\theta) = 0$ has a unique solution $\theta = \theta_1 \in (0, \frac{\pi}{2})$, where θ_1 is determined by (29). It is easy to show that $\tan \theta_1 > 1$, i.e. $\theta_1 \in (\frac{\pi}{4}, \frac{\pi}{2})$. The two trivial solutions agree with that discussed in Sec. 2 the u -axis is invariant, and that $\frac{du}{dt} \rightarrow 0^+$ and $\frac{dv}{dt} \rightarrow -\infty$ as $u \rightarrow 0^+$, implying that the trajectories of system (2) cannot cross the u -axis and v -axis. Hence, we

have

$$G(\theta) \begin{cases} > 0, & \text{for } 0 < \theta < \theta_1, \\ < 0, & \text{for } \theta_1 < \theta < \frac{\pi}{2}. \end{cases} \tag{31}$$

Further, we use the formula,

$$\frac{dr}{d\theta} = r \frac{H(\theta) + o(1)}{G(\theta)}, \quad \text{as } r \rightarrow 0, \tag{32}$$

where

$$\begin{aligned} H(\theta) &= \sin \theta V_3(\cos \theta, \sin \theta) + \cos \theta U_3(\cos \theta, \sin \theta) \\ &= -[1 + (a + 1)c] \cos^4 \theta \\ &\quad - \sin \theta \cos^3 \theta [m + a + (a - 1)c] \\ &\quad + c(2a + 1) \cos^2 \theta + c(a - 1) \sin \theta \cos \theta - ac \\ &= -\cos^4 \theta \{ m \tan \theta + [c \tan^2 \theta (\tan \theta - 1) + 1] \\ &\quad \times (a \tan \theta + 1) \}. \end{aligned} \tag{33}$$

It is obvious that

$$H(\theta) < 0, \quad \text{for } \theta_1 \leq \theta < \frac{\pi}{2}, \quad \text{due to } \theta_1 \in \left(\frac{\pi}{4}, \frac{\pi}{2}\right).$$

In addition, we have

$$\begin{aligned} G(\theta) &= -\sin \theta \cos^3 \theta \\ &\quad \times \{ \sqrt{[m + a + (a - 1)c]^2 + 4ac(1 + c)} \\ &\quad \times (\tan \theta - \tan \theta_1) + o(|\tan \theta - \tan \theta_1|) \} \\ &= -[\sin \theta_1 \cos^3 \theta_1 + O(|\theta - \theta_1|)] \\ &\quad \times \{ \sqrt{[m + a + (a - 1)c]^2 + 4ac(1 + c)} \\ &\quad \times (\theta - \theta_1) + o(|\theta - \theta_1|) \} \\ &= C(\theta - \theta_1) + o(|\theta - \theta_1|), \end{aligned} \tag{34}$$

where

$$\begin{aligned} C &= -\sin \theta_1 \cos^3 \theta_1 \\ &\quad \times \sqrt{[m + a + (a - 1)c]^2 + 4ac(1 + c)} \\ &< 0. \end{aligned} \tag{35}$$

Now applying Theorem 3.4 in [Zhang et al., 1991] with $k = 1, l = 1, C < 0$ and $H(\theta_1) < 0$ proves that any orbit tending to the origin must be along the direction $\theta = \theta_1$. Moreover, in the sector $\theta_1 < \theta < \frac{\pi}{2}$ near the origin, it follows from $G(\theta) < 0$ and $H(\theta) < 0$ that all orbits will move to the origin along the direction $\theta = \theta_1$. For the sector $0 < \theta < \theta_1$ near the origin, on the other hand, $G(\theta) > 0$, but

$H(\theta)$ is not necessarily less than 0. Nevertheless, we can show that the following holds:

- either (a) $H(\theta) < 0$ for $0 < \theta < \theta_1$
- or (b) $H(\theta_3) = H(\theta_2) = 0$ ($\theta_3 < \theta_2$)

such that

$$H(\theta) < 0 \quad \text{for } \theta \in (0, \theta_3) \cup (\theta_2, \theta_1) \quad \text{and}$$

$$H(\theta) > 0 \quad \text{for } \theta \in (\theta_3, \theta_2).$$

The special case $\theta_3 = \theta_2$ (a repeated root) can be included in the case (a). For the case (a), it is obvious that all orbits in the sector $0 < \theta < \theta_1$ will move to the origin along the direction $\theta = \theta_1$. For the case (b), due to the continuity of solutions, all orbits in the sector $0 < \theta < \theta_1$ will also move to the origin along the direction $\theta = \theta_1$.

To prove the existence of θ_3 and θ_2 , we consider the function in the script bracket of $H(\theta)$, denoted by

$$H_1(w) = mw + [cw^2(w - 1) + 1](aw + 1),$$

where

$$w = \tan \theta,$$

which is a fourth-degree polynomial in w . We need to determine the number of roots of $H_1(w)$ in $0 < w < 1$. It is easy to show that

$$\lim_{w \rightarrow \pm\infty} H_1(w) = \infty, \quad H_1\left(-\frac{1}{a}\right) = -\frac{m}{a},$$

$$H_1(0) = 1, \quad H_1(1) = m + a + 1,$$

$$\left. \frac{dH_1}{dw} \right|_{w=0} = m + a,$$

$$\left. \frac{dH_1}{dw} \right|_{w=1} = m + a + (a + 1)c,$$

$$\left. \frac{d^2H_1}{dw^2} \right|_{w=0} = -2c, \quad \left. \frac{d^2H_1}{dw^2} \right|_{w=1} = 2(3a + 2),$$

which indicates that $H_1(w)$ has two real roots in $w \in (-\infty, 0)$, and may have no roots, corresponding to the case (a), or two roots in $0 < w < 1$, corresponding to the case (b). To have two roots of $H_1(w)$ in $0 < w < 1$, the necessary condition is

$$H_2(w) \triangleq cw^2(w - 1) + 1 < 0.$$

It is easy to see that $H_2(w)$ reaches its minimal value at $w = \frac{2}{3}$, given by $H_2(\frac{2}{3}) = 1 - \frac{4c}{27}$. Hence,

when $c \leq \frac{27}{4}$, $H_1(w) > 0$ for $0 < w < 1$, and so $H(\theta) < 0$ for $0 < \theta < \frac{\pi}{4}$, leading to the case (a). When $c > \frac{27}{4}$, we have

$$H_1\left(\frac{2}{3}\right) = \frac{2}{3} \left[m - \left(a + \frac{3}{2} \right) \left(\frac{4c}{27} - 1 \right) \right].$$

Thus, for $c > \frac{27}{4}$ and $m \geq (a + \frac{3}{2})(\frac{4c}{27} - 1)$, $H_1(w) > 0$ for $0 < w < 1$, which again leads to the case (a). For $c > \frac{27}{4}$ and $m < (a + \frac{3}{2})(\frac{4c}{27} - 1)$, we have $H_1(\frac{2}{3}) < 0$, and then there are two roots $0 < w_3 = \tan(\theta_3) < w_2 = \tan(\theta_2) < 1$ such that $H_1(w_3) = H_1(w_2) = 0$, yielding $H_1(w) > 0$ for $w \in (0, w_3) \cup (w_2, 1)$ and $H_1(w) < 0$ for $w \in (w_3, w_2)$. This leads to the case (b).

Summarizing the above discussions proves Theorem 3. ■

As an illustration of Theorem 3 we present two examples by taking the following parameter values:

Example 1

$$a = \frac{1}{10}, \quad b = \frac{1}{10}, \quad m = \frac{11}{5}, \quad c = \frac{27}{20},$$

$$\tan \theta_1 = \frac{217 + \sqrt{97849}}{54} \Rightarrow \theta_1 \approx 1.4692234$$

$$\approx 84.18^\circ,$$

$$\frac{3267}{1600} = m_* < m < m_H,$$

$$m_H = \frac{257125 + 1331\sqrt{21553}}{204800} < m^* = \frac{891}{400},$$

$$\frac{9}{10} = 1 - b < c < c_u = \frac{81}{44}, \quad b < \frac{1}{4a + 5} = \frac{5}{27},$$

$$u_{3+} = v_{3+} = \frac{3}{5}.$$

Example 2

$$a = 3, \quad b = \frac{1}{10}, \quad m = 1, \quad c = 10,$$

$$m < m^* = \frac{81}{10} \left(< m_* = \frac{562}{45} \right), \quad c > c_u = \frac{81}{160},$$

$$u_{3+} = v_{3+} = \frac{11 + 4\sqrt{71}}{20},$$

$$\tan \theta_1 = \frac{675 + \sqrt{1368537}}{1596} \Rightarrow \theta_1 \approx 1.155918$$

$$\approx 66.23^\circ,$$

$$\tan \theta_2 = 0.812892 \Rightarrow \theta_2 \approx 0.682553 \approx 39.11^\circ,$$

$$\tan \theta_3 = 0.479461 \Rightarrow \theta_3 \approx 0.447082 \approx 25.62^\circ.$$

By Theorem 2, it is seen that the equilibrium E_{3+} is asymptotically stable for both the examples, but the first example has Hopf bifurcation occurring at $m = m_H$, leading to an unstable limit cycle as shown in Fig. 4(a) (belonging to the case (iii) in Theorem 2), while the second example does not have Hopf bifurcation (belonging to the case (i) in Theorem 2). The simulated phase portraits for the first example are shown in Figs. 3(a) and 3(b), and that for the second example is depicted in Fig. 3(c), where the blue lines in Figs. 3(a) and 3(c) denote the direction $\theta = \theta_1$, and the green lines in Fig. 3(c) represent the directions $\theta = \theta_3$ and $\theta = \theta_2$. Note that the diagram in Fig. 3(c) purposely makes a perfect square so one can observe from this figure

that the trajectories in the sector $\theta_3 < \theta < \theta_2$ are slightly increasing, i.e. $\frac{dr}{d\theta} > 0$.

Now, based on boundedness property (Theorem 1) and the local attraction of the origin (Theorem 3), it is easy to obtain the following corollaries.

Corollary 4.1. *The equilibrium E_0 (the origin) of system (2) is globally asymptotically stable in the region*

$$\Omega_1 = \{(u, v) \mid 0 < u \leq b, v > 0\}$$

for any $\gamma \in \Gamma_4$.

Proof. First, by Theorem 1, we know that all solution trajectories of system (2) converge to the trapping region Ω_0 . Note that on the line $u = b, \dot{x} < 0$, implying that all trajectories of system (2) moves into the region Ω_1 . Also note that in the region Ω_1 there are only two boundary equilibria E_0 and E_2 ,

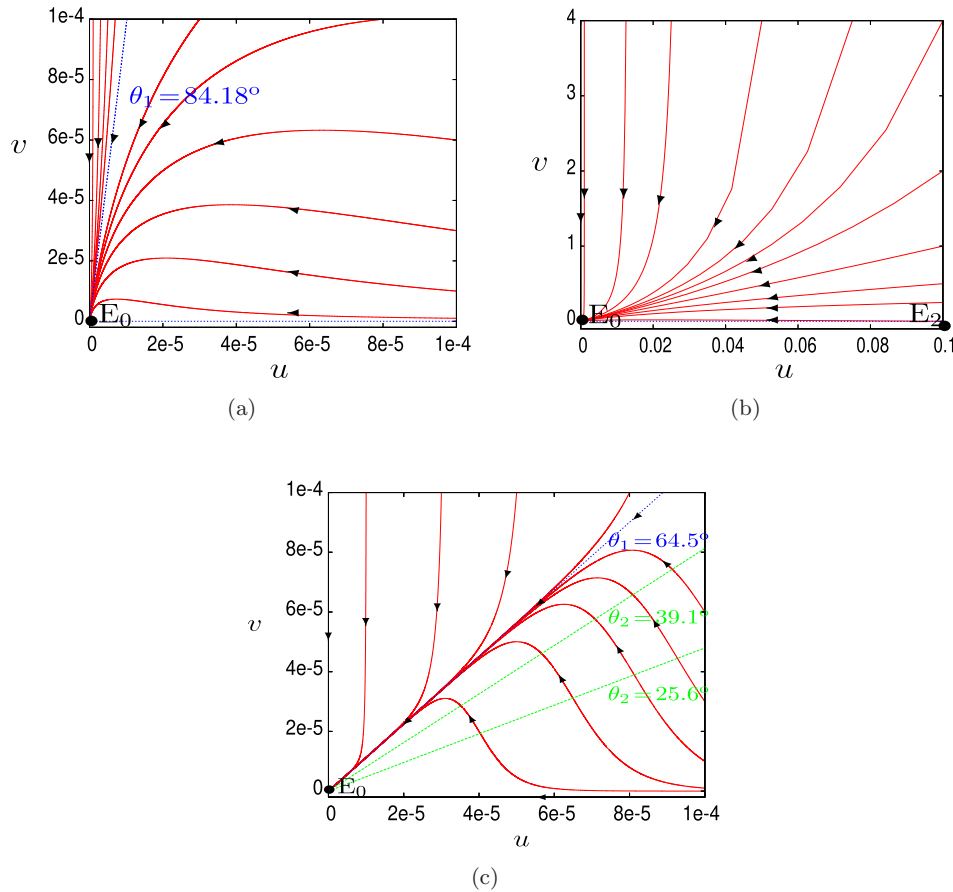


Fig. 3. Simulated phase portraits in the neighborhood of the origin of system (2) in I^+ of the u - v plane for (a) Example 1 $a = b = \frac{1}{10}, c = \frac{27}{20}$ and $m = \frac{11}{5}$, showing the local attraction of $(0, 0)$; (b) showing the global attraction of $(0, 0)$ for Example 1 in the region $\{(u, v) \mid 0 < u < b, v > 0\}$; and (c) Example 2 $a = 3, b = \frac{1}{10}, c = 10$ and $m = 1$, showing the local attraction of $(0, 0)$.

but E_2 is an unstable node. Thus, by Theorem 3, the only stable equilibrium in the region Ω_1 is E_0 . Therefore, any solution trajectory starting from an initial point in the region Ω_1 will eventually converge to E_0 . ■

Corollary 4.2. *The equilibrium E_0 (the origin) of system (2) is globally asymptotically stable in I^+ if $m > m^*$.*

Proof. The proof is similar to that for Corollary 4.1. When $m > m^*$, the equilibria E_3 or $E_{3\pm}$ do not exist, and the two boundary equilibria E_1 and E_2 are unstable. Thus, in the whole region I^+ , the only stable equilibrium is the origin. By Theorems 1 and 3 we know that any solution of system (2) starting in I^+ will eventually converges to E_0 . ■

In the following, we discuss more complex cases when $m \leq m^*$. We have several results on the global property of solutions of system (2). For convenience, we use the following notations:

$$\begin{aligned} &\Gamma_{E_2E_{3-}}, \quad \Gamma_{E_2E_3}, \quad \Gamma_{E_0E_1}, \quad \Gamma_{E_1E_{3-}}, \\ &\Gamma_{E_1E_{3+}}, \quad \Gamma_{E_0E_3}, \quad \Gamma_{E_0E_{3-}}, \quad \Gamma_{E_{3-}E_{3+}}, \end{aligned}$$

where, for example, $\Gamma_{E_2E_{3-}}$ denotes the heteroclinic orbit connecting the unstable node E_2 and the saddle E_{3-} , and similar definitions for others.

Proposition 1. *Assume that $m < m^*$ for system (2). Then, there exists $\Gamma_{E_2E_{3-}}$ joining the equilibria E_2 and E_{3-} .*

Proof. First, we prove that on the line segment $u = u_{3-}, 0 < v < v_{3-}, \dot{u} > 0$ and $\dot{v} > 0$, since

$$\begin{aligned} \dot{u} &= u_{3-} \left[\frac{1}{b}(1 - u_{3-})(u_{3-} - b) - \frac{mv}{u_{3-} + av} \right] \\ &= u_{3-} \left[\frac{1}{b}(1 - u_{3-})(u_{3-} - b) - \frac{mv_{3-}}{u_{3-} + av_{3-}} \right. \\ &\quad \left. + \frac{mv_{3-}}{u_{3-} + av_{3-}} - \frac{mv}{u_{3-} + av} \right] \\ &= -\frac{mu_{3-}(v - v_{3-})}{(a + 1)(u_{3-} + av)} > 0, \\ \dot{v} &= cu_{3-} \left(1 - \frac{v}{u_{3-}} \right) = cu_{3-} \left(1 - \frac{v}{v_{3-}} \right) > 0. \end{aligned} \tag{36}$$

Since E_{3-} is a saddle point, we need to prove that the slope, s_1 , of the tangent line to the stable manifold of E_{3-} is larger than 1 ($s_1 > 1$), that is, the trajectory moving into E_{3-} must be below the line $v = u$; and the slope, s_2 , of the tangent line to the unstable manifold of E_{3-} is smaller than 1 ($0 < s_2 < 1$), that is, the trajectory moving out E_{3-} must be above the line $v = u$. Therefore, there must exist a heteroclinic orbit $\Gamma_{E_2E_{3-}}$ joining E_2 and E_{3-} , rather than connecting E_1 and E_{3-} . In other words, the heteroclinic orbit $\Gamma_{E_1E_{3-}}$ cannot connect E_{3-} from below if it exists. Otherwise, suppose $\Gamma_{E_1E_{3-}}$ connects E_{3-} from below, then the trajectories below E_{3-} and near the line segment $u = u_{3-}, 0 < v < v_{3-}$ must cross this line segment from the left to the right and then have to go back to cross this same line segment again from the right to the left due to the uniqueness of solutions (avoiding intersection with the curve connecting E_1 and E_{3-}). But this is obviously impossible, as seen from Fig. 4.

With the variation of the parameter c , it is observed from Fig. 4 that a heteroclinic orbit not only exists between the unstable node E_2 and the saddle E_{3-} ($\Gamma_{E_2E_{3-}}$), but also exists between the saddle E_1 and the degenerate stable node E_0 ($\Gamma_{E_0E_1}$), or between the saddle E_1 and the stable focus E_{3-} ($\Gamma_{E_1E_{3-}}$), or between the saddle E_1 and the stable focus E_{3+} ($\Gamma_{E_1E_{3+}}$), depending upon the values of c . One can use Theorem 2 to verify that E_{3+} is AS for all the values of c taken in the four diagrams in Fig. 4. In fact, for the parameter values $a = b = 0.1, m = 2.2$, the critical value of c for E_3 becomes unstable at $c \approx 1.218182$. Taking $c = 1.15$ we will get a similar diagram as that in Fig. 4(a), which has unstable focus E_{3+} and no limit cycle, and still has the heteroclinic orbit connecting the saddle E_1 and the degenerate stable node E_0 ($\Gamma_{E_0E_1}$). This implies that there exists a critical value of $c = c^*$, when a, b and m are fixed, such that $\Gamma_{E_0E_1}$ exists for $c < c^*$, $\Gamma_{E_1E_{3-}}$ exists for $c = c^*$, and $\Gamma_{E_1E_{3+}}$ exists for $c > c^*$. For $a = b = 0.1, m = 2.2, c^* = 1.8277664183$. But the heteroclinic orbit $\Gamma_{E_2E_{3-}}$ always exists for any $\gamma \in \Gamma_4$.

Now, we prove the properties mentioned above about the stable and unstable manifolds of E_{3-} . Let J_{3-} be the Jacobian of system (2) evaluated at E_{3-} , denoted by

$$J(E_{3-}) = \begin{bmatrix} p_{11} + p_{12} & -p_{12} \\ c & -c \end{bmatrix}, \tag{36}$$

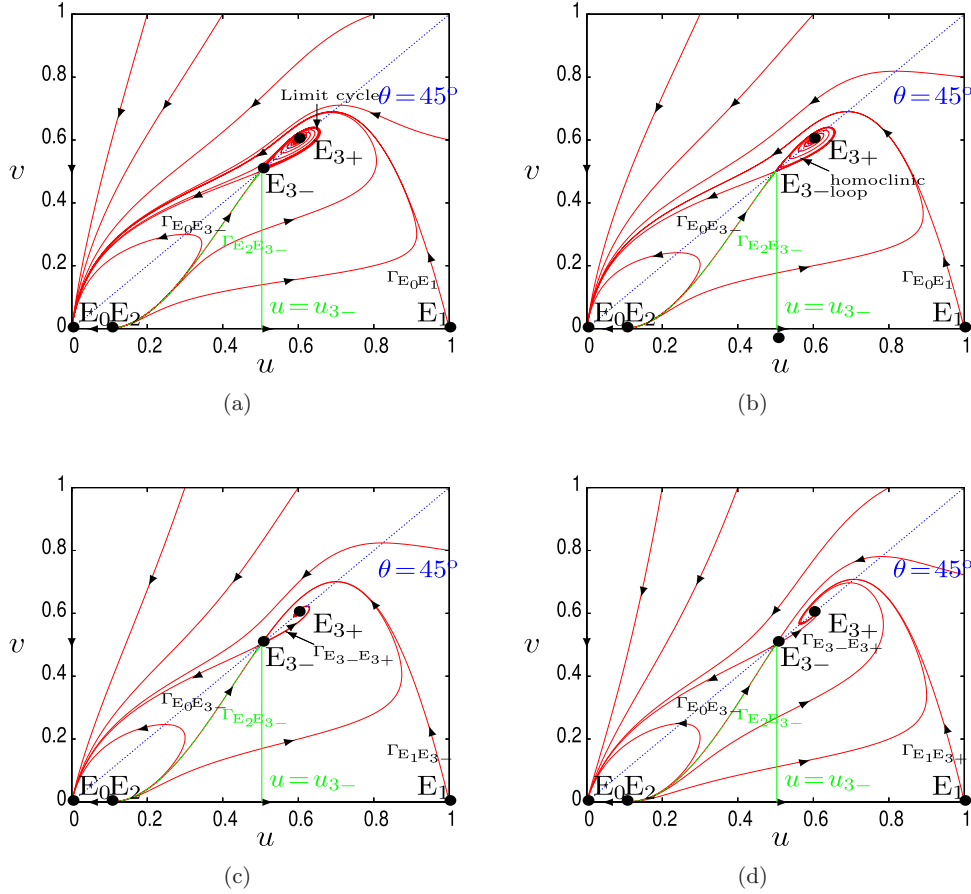


Fig. 4. Simulated phase portraits of system (2) with $a = b = 0.1$, $m = 2.2$, showing a heteroclinic orbit connecting the unstable node E_2 and the saddle E_{3-} (E_{3+} being a stable focus) with different topological structures: (a) $c = 1.35$ yielding an unstable limit cycle from a subcritical Hopf bifurcation; (b) $c = 1.3660350289$ yielding an unstable homoclinic loop; (c) $c = 1.8277664183$ yielding another heteroclinic orbit connecting the two saddles E_1 and E_{3-} ; and (d) $c = 2.2$ yielding another heteroclinic orbit connecting the saddle E_1 and the stable focus E_{3+} . The green curve is the orbit connecting the equilibria E_2 and E_{3-} , and the green vertical line is the line segment $u = u_{3-}$, $0 < v < v_{3-}$.

where

$$p_{11} = \frac{1}{b} \sqrt{\frac{b}{a+1}} (m^* - m) \times \left[1 + b - \sqrt{(1-b)^2 - \frac{4mb}{a+1}} \right] > 0 \quad \text{and}$$

$$p_{12} = \frac{m}{(a+1)^2} > 0,$$

for $m < m^*$. Then,

$$\text{Tr}(J(E_{3-})) = p_{11} + p_{12} - c,$$

and

$$\det(J(E_{3-})) = -cp_{11} < 0$$

(which is the same as that given in Theorem 2). The two eigenvalues of $J(E_{3-})$ are given by

$$\lambda_1 = \frac{1}{2} [\text{Tr}(J(E_{3-})) - \sqrt{\text{Tr}(J(E_{3-}))^2 - 4 \det(J(E_{3-}))}] < 0,$$

$$\lambda_2 = \frac{1}{2} [\text{Tr}(J(E_{3-})) + \sqrt{\text{Tr}(J(E_{3-}))^2 - 4 \det(J(E_{3-}))}] > 0,$$

and the corresponding eigenvectors are

$$v_1 = (c + \lambda_1, c)^T, \quad v_2 = (c + \lambda_2, c)^T.$$

It is obvious that the slope of the eigenvector v_2 equals $s_2 = \frac{c}{c + \lambda_2}$ satisfying $s_2 \in (0, 1)$. For the

eigenvector v_1 , its slope is equal to $s_1 = \frac{c}{c+\lambda_1}$. A direct computation yields that

$$\begin{aligned} c + \lambda_1 &= \frac{1}{2}[\text{Tr}(J(E_{3-})) + 2c - \sqrt{\text{Tr}(J(E_{3-}))^2 - 4 \det(J(E_{3-}))}] \\ &= \frac{2cp_{12}}{p_{11} + p_{12} + c + \sqrt{p_{11}(p_{11} + 2p_{12} + 2c) + (p_{12} - c)^2}} \\ &> 0, \end{aligned}$$

which implies that $s_1 \in (1, \infty)$. This can be seen from Fig. 4 where the green curve is the heteroclinic orbit $\Gamma_{E_2E_{3-}}$, and the green vertical line is the line segment $u = u_{3-}$, $0 < v < v_{3-}$.

The proof is finished. ■

Proposition 2. Assume that $m = m^*$ for system (2). Then, the positive equilibrium $E_3 = (u_3, v_3)$ of this system is a cusp point of order two.

Proof. Eliminating m from the two equations: $\dot{u} = \dot{v} = 0$, we obtain the solution for m and a resultant as follows:

$$\begin{aligned} m &= \frac{(1-u)(u-b)(u+av)}{bv}, \\ R_{23} &= cv(u-v)(u+av). \end{aligned}$$

It is obvious that the nonzero solution to $R_{23} = 0$ is $v = u$. Using $R_{23} = 0$, we find

$$\begin{aligned} \frac{dv}{du} &= -\frac{\frac{\partial R_{23}}{\partial u}}{\frac{\partial R_{23}}{\partial v}} = \frac{av(3v-2u) + u(2v-u)}{v(2u-v+av)} \\ &\Rightarrow \left. \frac{dv}{du} \right|_{v=u} = 1, \end{aligned}$$

which shows that the orbits connecting E_3 have a common tangent line, implying that E_3 is a cusp point of order two. Moreover, note that this common tangent line has a constant slope 1 for any parameter value. It is easy to verify that $m = m^*$ at $E_3 = (\frac{1}{2}(1+b), \frac{1}{2}(1+b))$. ■

Theorem 4. Assume that $m < m^*$ for system (2). Then, $\lim_{t \rightarrow \infty} (u(t), v(t)) = (0, 0)$ when $u_0 \leq \min\{u_{3-}, v_0\}$ and $(u_0, v_0) \neq (u_{3-}, v_{3-})$.

Proof. This is equivalent to proving that the trajectories of system (2) starting from any initial points in the region Ω_2 converges to $(0, 0)$, where Ω_2 is

defined as

$$\Omega_2 = \{(u, v) \mid v \geq u, 0 \leq u \leq u_{3-}\}.$$

In other words, Ω_2 is bounded by the v -axis, and the lines $u = v$ and $u = u_{3-}$. By Theorems 1 and 3, we only need to show that the trajectories of system (2) move into Ω_2 when they pass through the two lines $u = v$ and $u = u_{3-}$.

On the line $u = v$, it is obvious that $\dot{v} = 0$, and it is easy to obtain that

$$\begin{aligned} \dot{u} &= u \left[\frac{1}{b}(1-u)(u-b) - \frac{mu}{u+au} \right] \\ &= -\frac{u}{b} \left[u^2 - (1+b)u + b \left(1 + \frac{m}{a+1} \right) \right] \\ &< 0, \end{aligned}$$

for $0 < u < u_{3-}$ since the term in the square bracket is the polynomial F_1 in (2), and u_{3-} is the smaller positive root of F_1 .

On the line segment $u = u_{3-}$, $v > v_{3-}$, similar to the proof for Proposition 1, we can use (36) to show that $\dot{u} < 0$ and $\dot{v} < 0$, which implies that Ω_2 is invariant and thus the conclusion of Theorem 4 is true. ■

It should be pointed out that the conclusion in Theorem 4 is conservative. It can be seen from Fig. 4 that the trapping region Ω_2 can be defined larger, but then the definition will depend on the parameter values, making it more complex. While the conclusion in Theorem 4 is independent of the parameters (i.e. it is true for any $\gamma \in \Gamma_4$).

Theorem 5. Assume that $m = m^*$ for system (2). Then, $\lim_{t \rightarrow \infty} (u(t), v(t)) = (0, 0)$ provided that $(u_0, v_0) \notin \Gamma_{E_2E_3}$.

Proof. By Proposition 2, we know that the equilibrium $E_3 = (u_3, v_3)$ of system (2) is a cusp point of order two when $m = m^*$. Then, similar to the proof for Proposition 1, we consider the dynamics on the

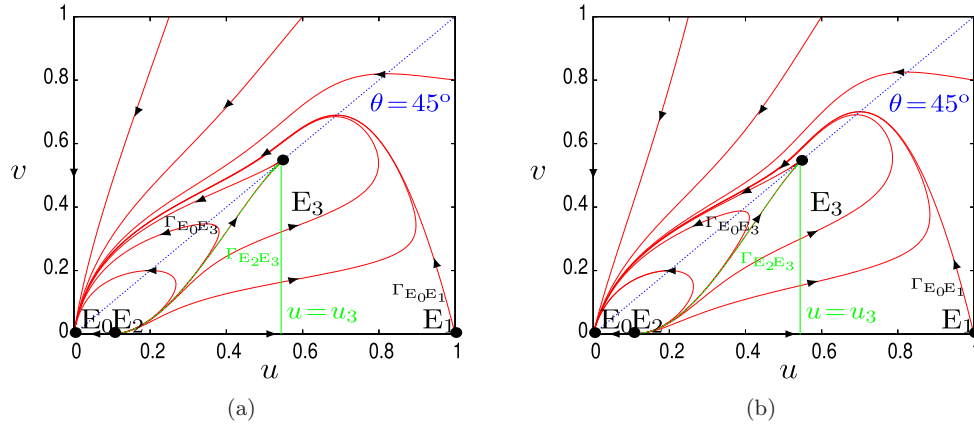


Fig. 5. Simulated phase portraits of system (2) for $a = b = 0.1$, $m = m^* = 2.2275$, showing that the equilibrium E_3 is a cusp point of order two: (a) $c = 1.5 < c_u \approx 1.8409$; and (b) $c = 2 > c_u$. The green orbit $\Gamma_{E_2E_3}$ connects E_2 and E_3 , and the green vertical line is the line segment $u = u_3$, $0 < v < v_3$.

line segment $u = u_3$, $0 < v < v_3$ to obtain $\dot{v} > 0$ and that

$$\begin{aligned} \dot{u} &= u_3 \left[\frac{1}{b}(1 - u_3)(u_3 - b) - \frac{mv}{u_3 + av} \right] \\ &= u_3 \left[\frac{1}{b}(1 - u_3)(u_3 - b) - \frac{mv_3}{u_3 + av_3} \right. \\ &\quad \left. + \frac{mv_3}{u_3 + av_3} - \frac{mv}{u_3 + av} \right] \\ &= \frac{mu_3(v_3 - v)}{(a + 1)(u_3 + av)} \\ &> 0, \quad \text{for } v < v_3, \end{aligned}$$

which indicates that the trajectories passing through the line segment $u = u_3$, $0 < v < v_3$ must be from the left to the right. Also, note that the trajectory moving to the cusp point (the stable manifold of E_3) must be below the line $v = u$, while the trajectory leaving the cusp point (the unstable manifold of E_3) must be above the line $v = u$. Since $E_1 = (1, 0)$ is a saddle point, and $E_2 = (b, 0)$ is an unstable node, and note that $b < u_3 < 1$, there must exist an orbit connecting E_2 and E_3 , rather than connecting E_1 and E_3 . Otherwise, there are at least two trajectories moving into the cusp point. Hence, a trajectory starting from any $(u_0, v_0) \notin \Gamma_{E_2E_3}$ must converge to $E_0 = (0, 0)$ since in this case the origin is the unique stable equilibrium in I^+ . ■

Two illustrative examples showing the cusp point E_3 are given in Fig. 5 for which the parameter values are taken as $a = b = 0.1$, $m = m^* = 2.2275$,

and $c = 1.5$ for Fig. 5(a) and $c = 2$ for Fig. 5(b), with $c_u = \frac{81}{44} \approx 1.8409$. In the figure, the green curve is the heteroclinic orbit $\Gamma_{E_2E_3}$, and the green vertical line is the line segment $u = u_3$, $0 < v < v_3$. It is seen from the figure that the cusp point E_3 does not change its topological structure regardless whether $c < c_u$ or $c > c_u$, which implies that it is irrelevant to the dynamics on the center manifold (see Theorem 2).

In summary, we have shown in this section that if system (2) has no positive equilibria, then all trajectories in I^+ converge to $(0, 0)$ and $(0, 0)$ is globally asymptotically stable. If system (2) has two positive equilibria $E_{3\pm}$, then when the initial value of the prey u with strong Allee effect is smaller than that of predator, the solution trajectories converge to $(0, 0)$, implying that both predator and prey will become extinct under these situations. On the contrary, when the initial value of the prey with strong Allee effect is bigger than that of predator, the situation becomes complicated. Namely, the population of a species will coexist, die out or tend to periodic fluctuations [Lu et al., 2021]. If system (2) has only one positive equilibrium E_3 , then almost all the solutions of the system converge to $(0, 0)$, except one orbit connecting the equilibria E_2 and E_3 , implying that both predator and prey will almost become extinct in this situation.

5. Bifurcation Analysis

This section is devoted to further bifurcation analysis on the equilibrium solutions of system (2). Our particular attention is focused on the bifurcations

of the interior equilibrium, including saddle-node bifurcation, Hopf bifurcation and BT bifurcation.

5.1. Saddle-node bifurcation

In this section, we apply center manifold theory to derive the conditions for the saddle-node bifurcation of system (2) which occurs from the positive equilibrium E_3 at

$$m = m^* = \frac{(a+1)(1-b)^2}{4b},$$

with $c \neq c_u = \frac{(1-b)^2}{4b(a+1)}$. We have the following result.

$$\begin{cases} \dot{x}_1 = -\frac{c(1+b)}{4b(a+1)(c-c_u)} \left[2b\mu + 2(a+1)x_1^2 + \frac{(1-b)^2}{b}x_1x_2 + \frac{(1-b)^2}{b}x_1\mu \right. \\ \quad \left. + \frac{4bc(a+1) + a(1-b)^2}{(a+1)^2(1+b)}x_2\mu + \dots \right], \\ \dot{x}_2 = -(c-c_u)x_2 + \frac{(1+b)}{4b(a+1)(c-c_u)} \left[2b\mu + 2(a+1)x_1^2 + \frac{(1-b)^2}{b}x_1x_2 + \frac{4b}{1+b}x_1\mu \right. \\ \quad \left. + \frac{4bc(a+1) + a(1-b)^2}{(a+1)^2(1+b)}x_2\mu + \dots \right]. \end{cases}$$

Assume the center manifold is given by $x_2 = h_{20}x_1^2 + h_{11}x_1\mu + h_{02}\mu^2$. Then, using $\dot{x}_2 = (2h_{20}x_1 + h_{11}\mu)\dot{x}_1$ together with the above equations we find the center manifold CM_μ and the differential equation describing the dynamics on the CM_μ :

$$\dot{x}_1 = -\frac{2bc(1+b)}{4b(a+1)(c-c_u)} \left[\mu + \frac{(a+1)}{b}x_1^2 + \frac{2}{1+b}x_1\mu + \dots \right],$$

which clearly shows that the saddle-node bifurcation occurs when m is varied to pass through the critical point $m = m^*$ with $c \neq c_u$. No transcritical bifurcation or pitchfork bifurcation can happen. ■

It follows from (15) that when m crosses the critical point $m = m^*$, the number of equilibrium solutions changes from zero to two, or from two to zero. When $m = m^*$ and $c = c_u$, BT bifurcation occurs, which will be discussed in Sec. 5.3

5.2. Hopf bifurcation

The detailed linear analysis on Hopf bifurcation has been given in Sec. 3 with the Hopf critical point m_H given in (16). In this section, we will consider the limit cycles arising from the Hopf bifurcation. In particular, we want to ask: What is the codimension of the Hopf bifurcation? That is, what is maximal number of limit cycles which can cause bifurcation

Theorem 6. System (2) undergoes a saddle-node bifurcation from the equilibrium $E_3 = (u_3, u_3) = (\frac{1}{2}(1+b), \frac{1}{2}(1+b))$ at the critical point $m = m^*$ with $c \neq c_u$.

Proof. In Sec. 3 we have applied center manifold theory to find the center manifold CM (20) at the critical point $m = m^*$ and the differential equation (21) on the CM. Now, we want to find the center manifold and associated differential equation on the center manifold under the perturbation of m . Let $m = m^* + \mu$. Then, using the transformation (19), we obtain

from the equilibrium E_{3+} at the critical point m_H ? We will show that the Hopf bifurcation is subcritical, and the bifurcating limit cycle is unstable, since the first focus value $v_1 > 0$ for any $\gamma \in \Gamma_4$. In other words, the codimension of the Hopf bifurcation is one. We have the following theorem.

Theorem 7. The model (2) undergoes Hopf bifurcation from the positive equilibrium E_{3+} , yielding an unstable limit cycle. The codimension of the Hopf bifurcation is one.

Proof. In order to calculate the first focus value v_1 , instead of u , we use the parameter m to solve the polynomial equation $F_1 = 0$ to obtain

$$m = \frac{a+1}{b}(1-u_3)(u_3-b), \tag{37}$$

which requires

$$b < u_3 < 1, \quad \text{due to } m > 0. \tag{38}$$

We then use the parameter c to solve the trace equation $\text{Tr}(J(E_3)) = 0$ to obtain

$$c_H = -\frac{1}{b(a+1)}[(2a+3)u_3^2 - (a+2)(b+1)u_3 + b], \tag{39}$$

where c_H indicates the Hopf critical point. To have $c_H > 0$, it needs $0 < u_{3-} < u_3 < u_{3+}$, where

$$u_{3\pm} = \frac{1}{2(2a+3)}[(a+2)(b+1) \pm \sqrt{a^2(b+1)^2 + 4a(b^2+1) + 4(1-b+b^2)}].$$

It can be shown that $u_{3-} < b < u_{3+} < 1$. Thus, we have the restrict condition on u_3 :

$$b < u_3 < u_{3+}. \tag{40}$$

$$\begin{pmatrix} u \\ v \end{pmatrix} = \begin{pmatrix} u_3 \\ u_3 \end{pmatrix} + \begin{bmatrix} 1 & 0 \\ \frac{b(a+1)c_H}{(1-u_3)(u_3-b)} & \frac{b\omega_c}{(a+1)u_3^2(1-u_3)(u_3-b)} \end{bmatrix} \begin{pmatrix} x_1 \\ x_2 \end{pmatrix}, \tag{43}$$

into system (2) to obtain the system

$$\begin{cases} \dot{x}_1 = \omega_c x_2 + \frac{(a+1)x_3^2[(4a+3)x_3^3 - 4(b+1)(a+1)x_3^2 + ((a+1)b^2 + (2a+5)b + a+1)x_3 - b(1+b)]}{b(1-x_3)(x_3-b)} x_1^2 \\ \quad + \frac{\omega_c[2(a-1)x_3^2 + (2-a)(b+1)x_3 - 2b]}{x_3(1-x_3)(x_3-b)} x_1 x_2 + \dots, \\ \dot{x}_2 = -\omega_c x_1 + \frac{\omega_c[(12a+11)x_3^3 - 2(1+b)(6a+7)x_3^2 + ((3a+4)b^2 + 3(2a+5)b + 3a+4)x_3 - 3b(1+b)]}{x_3(2x_3-1-b)(1-x_3)(x_3-b)} x_1^2 \\ \quad + \frac{\omega_c^2 b(5a+2)}{x_3^3(a+1)(1-x_3)(x_3-b)} x_1 x_2 + \frac{\omega_c^3 b^2(2a+1)}{x_3^6(2x_3-1-b)(a+1)^2(1-x_3)(x_3-b)} x_2^2 + \dots, \end{cases} \tag{44}$$

whose linear part is in the Jordan canonical form,

$$J(0,0) = \begin{bmatrix} 0 & \omega_c \\ -\omega_c & 0 \end{bmatrix}.$$

Next, we apply the Maple program [Yu, 1998; Yu & Bi, 1998] for computing the normal form of Hopf and generalized Hopf bifurcation to system (44) to get the first focus value:

$$v_1 = -\frac{u_3}{8b(a+1)(2u_3-1-b)} \tilde{v}_1, \quad \text{where} \\ \tilde{v}_1 = 4a(a+4)u_3^2 - (b+1)(3a^2+16a+1)u_3 + 3a(b+1)^2. \tag{45}$$

At the critical point $c = c_H$, we obtain

$$\det(J(E_3)) = \frac{(a+1)^2 u_3^4}{b^2} [bu_3 c_H (2u_3 - 1 - b)],$$

which defines the critical frequency at the Hopf critical point as

$$\omega_c = \frac{(a+1)u_3^2}{b} \sqrt{bu_3 c_H (2u_3 - 1 - b)} \tag{41}$$

that needs $u_3 > \frac{1}{2}(1+b)$. Hence, the restrict condition (40) becomes

$$\frac{1}{2}(1+b) < u_3 < u_{3+}. \tag{42}$$

Now, we first multiply $u(u+av)$ to system (2) and then introduce the affine transformation,

Note that \tilde{v}_1 is a quadratic polynomial in u_3 , having the opposite sign as that of v_1 . In the following, we show that $\tilde{v}_1 < 0$ (i.e. $v_1 > 0$) for any $\gamma \in \Gamma_4$. To have bifurcation of multiple limit cycles, i.e. the codimension of the Hopf bifurcation is higher than one, v_1 must be equal to zero. Thus, solving $\tilde{v}_1 = 0$ yields two solutions:

$$u_3^\pm = \frac{1}{8a(a+4)} [(b+1)(3a^2+16a+1) \pm (a+1)(b+1)\sqrt{9a^2+30a+1}].$$

However, a direct computation shows that

$$u_3^+ - u_{3+} = 2(2a+3)[6(1+b)^2 a^5 + (35b^2+102b+35)a^4$$

$$\begin{aligned}
 &+ 64(b^2 + 6b + 1)a^3 + 2(13b^2 + 282b + 13)a^2 \\
 &+ 66(1 + b)^2a + 3(1 + b)^2 + (a + 1)^2(b + 1)^2 \\
 &\times (2a^2 + 15a + 3)\sqrt{9a^2 + 30a + 1}] > 0, \\
 &\frac{1}{2}(1 + b) - u_3^- \\
 &= (a + 1)(b + 1)[\sqrt{9a^2 + 30a + 1} + a - 1] > 0,
 \end{aligned}$$

implying that $u_3^- < \frac{1+b}{2} < u_{3+} < u_3^+$, namely, the two solutions u_3^\pm to $v_1 = 0$ are outside the feasible parameter interval $(\frac{1+b}{2}, u_{3+})$. Moreover, $\tilde{v}_1 < 0$ for $u_3 \in (\frac{1+b}{2}, u_{3+})$, and so $v_1 > 0$, indicating that the Hopf bifurcation is subcritical, and the bifurcating limit cycle is unstable. ■

5.3. Bogdanov–Takens bifurcation

In this section, we consider BT bifurcation. As shown in Sec. 3 BT bifurcation must happen at

$$\begin{aligned}
 m = m^* &= \frac{(a + 1)(1 - b)^2}{4b} \quad \text{from the equilibrium} \\
 E_3 = (u_3, v_3), \quad \text{with } u_3 = v_3 &= \frac{1}{2}(1 + b),
 \end{aligned}$$

at which $\det(J(E_3)) = 0$, and

$$\text{Tr}(J(E_3)) = \frac{1}{4b(1 + a)}[(1 - b)^2 - 4bc(1 + a)].$$

Then, solving $\text{Tr}(J(E_{3+})) = 0$ with $m = m^*$ yields

$$\begin{aligned}
 (1 - \bar{b})^2 - 4\bar{b}\bar{c}(1 + \bar{a}) &= 0, \\
 (1 + \bar{a})(1 - \bar{b})^2 - 4\bar{b}\bar{m} &= 0,
 \end{aligned} \tag{46}$$

where $(\bar{a}, \bar{m}, \bar{b}, \bar{c})$ represents the BT critical point at which the equilibrium is given by $E_3 = (\frac{1}{2}(1 + \bar{b}), \frac{1}{2}(1 + \bar{b}))$. The two equations in (46) may be solved by six combinations of choosing two parameters from the four parameters. In order to definitely determine the BT critical point, without loss of generality, one may solve \bar{a} and \bar{m} to obtain

$$\begin{aligned}
 \bar{a} &= \frac{(1 - \bar{b})^2 - 4\bar{b}\bar{c}}{4\bar{b}\bar{c}}, \\
 \bar{m} &= \frac{(1 - \bar{b})^4}{16\bar{b}^2\bar{c}}, \quad \left(\bar{c} < \frac{(1 - \bar{b})^2}{4\bar{b}}\right).
 \end{aligned} \tag{47}$$

The other five combinations lead to the same result.

Now, taking perturbation on the critical parameter values, we let

$$a = \bar{a} + \mu_1, \quad m = \bar{m} + \mu_2, \tag{48}$$

$$b = \bar{b} + \mu_3, \quad c = \bar{c} + \mu_4,$$

and introduce an affine transformation:

$$\begin{aligned}
 u &= \frac{1 + \bar{b}}{2} + \bar{c}x_1 + x_2, \\
 v &= \frac{1 + \bar{b}}{2} + \bar{c}x_1,
 \end{aligned} \tag{49}$$

into the original system (2) to obtain a new system up to second-order terms:

$$\left\{ \begin{aligned}
 \dot{x}_1 &= x_2 - \frac{2}{1 + \bar{b}}x_2^2 + O(|(x_1, x_2, \mu)|^3), \\
 \dot{x}_2 &= -\frac{\bar{c}^2(1 + \bar{b})}{2\bar{b}}x_1^2 - \frac{\bar{c}(1 + \bar{b})}{\bar{b}}x_1x_2 - \frac{(1 - \bar{b}^2 - 4\bar{b}\bar{c})^2 + 16\bar{b}^2\bar{c}(1 - \bar{b})}{2\bar{b}(1 + \bar{b})(1 - \bar{b})^2}x_2^2 + \frac{\bar{c}(1 + \bar{b})}{2}\mu_1 \\
 &\quad - \frac{2\bar{b}\bar{c}(1 + \bar{b})}{(1 - \bar{b})^2}\mu_2 - \frac{2\bar{b}\bar{c}^2(1 + \bar{b})}{(1 - \bar{b})^2}\mu_1^2 + \frac{8\bar{b}^2\bar{c}^2(1 + \bar{b})}{(1 - \bar{b})^4}\mu_1\mu_2 - \frac{(1 - \bar{b})(1 + \bar{b})^2}{8\bar{b}^2}\mu_3 \\
 &\quad + \frac{(1 - \bar{b})(1 + \bar{b})^2}{8\bar{b}^3}\mu_3^2 + \bar{c}^2\left(\mu_1 - \frac{4\bar{b}}{(1 - \bar{b})^2}\mu_2\right)x_1 + \frac{\bar{c}(1 + \bar{b})(3\bar{b} - 1)}{4\bar{b}^2}\mu_3x_1 \\
 &\quad + \bar{c}\left[\frac{(1 - \bar{b})^2 - 8\bar{b}\bar{c}}{(1 - \bar{b})^2}\mu_1 - \frac{4\bar{b}[(1 - \bar{b})^2 - 4\bar{b}\bar{c}]}{(1 - \bar{b})^4}\mu_2\right]x_2 + \left[\frac{(1 + \bar{b})(3\bar{b} - 1)}{4\bar{b}}\mu_3 - \mu_4\right]x_2 \\
 &\quad + O(|(x_1, x_2, \mu)|^3),
 \end{aligned} \right. \tag{50}$$

where $\mu = (\mu_1, \mu_2, \mu_3, \mu_4)$. To determine the codimension of the BT bifurcation, we let $\mu_1 = \mu_2 = \mu_3 = \mu_4 = 0$ in (50), which gives $\bar{a} = a, \bar{m} = m, \bar{b} = b, \bar{c} = c$, and take the following nonlinear transformation up to second order,

$$\begin{cases} x_1 = y_1 - \frac{(1-b^2-4bc)^2 + 16b^2c(1-b)}{4b(1+b)(1-b)^2} y_1^2, \\ x_2 = y_2 - \frac{(1-b^2-4bc)^2 + 16b^2c(1-b)}{2b(1+b)(1-b)^2} y_1 y_2 \\ \quad + \frac{2}{1+b} y_2^2, \end{cases} \quad (51)$$

into (50)| $\mu_1=\mu_2=0$ to obtain the normal form up to second-order terms:

$$\dot{y}_1 = y_2 + O(|(y_1, y_2)|^3),$$

$$\dot{y}_2 = C_{20} y_1^2 + C_{11} y_1 y_2 + O(|(y_1, y_2)|^3), \quad (52)$$

where

$$C_{20} = -\frac{c^2(1+b)}{2} < 0, \quad C_{11} = -\frac{c(1+b)}{b} < 0, \quad (53)$$

implying that the codimension of the BT bifurcation is two, which is usually called a cusp BT bifurcation.

Next, we want to find unfolding to the normal form (52). To get a general result, we keep μ (including the four perturbations) in the system, and take the relation in (47), which implies that \bar{b} and \bar{c} can be chosen arbitrary, leading to the simple notation $\bar{b} = b, \bar{c} = c$. Next, introducing the nonlinear state transformation

$$\begin{cases} x_1 = \frac{2b}{c^2(1+b)} y_1 + \frac{(1-b^2)^2 - 4bc[(1-b)^2 - 4bc]}{4c(1+b)(1-b)^2} \mu_1 - \frac{b\{(1-b^2)^2 - 4bc[(1-b)^2 - 4bc]\}}{c(1-b)^4(1+b)} \mu_2 \\ \quad - \frac{(1-b^2)^2 + 4bc(b^2 + 4bc - 1)}{16b^2c^2(1-b)} \mu_3 - Q(\mu)y_1 - \frac{(1-b^2)^2 - 8bc[(1-b)^2 - 2bc]}{c_4(1-b)^2(1+b)^3} y_1^2, \\ x_2 = \frac{2b}{c^2(1+b)} y_2 - Q(\mu)y_2 - \frac{2b\{(1-b^2)^2 - 8bc[(1-b)^2 - 2bc]\}}{c^4(1-b)^2(1+b)^3} y_1 y_2 + \frac{8b^2}{c^4(1+b)^3} y_2^2, \end{cases} \quad (54)$$

where

$$\begin{aligned} Q(\mu) = & \frac{(1-b^2)^4 - 16bc\{(1+b)^2(1-b)^4 - bc[3(3b^2 + 2b + 3)(1-b)^2 - 16bc((1-b)^2 - bc)]\}}{8c^3(1+b)^3(1-b)^4} \mu_1 \\ & - \frac{b\{(1-b^2)^2 - 4bc[(1-b)^2 - 4bc]\}\{(1-b^2)^2 - 4bc[3(1-b)^2 - 4bc]\}}{2c^3(1+b)^3(1-b)^6} \mu_2 \\ & - \frac{(1-b^2)^4 - 16bc[(1-b)^2 - bc][(1-b^2)^2 + 16b^2c^2]}{32b^2c^4(1+b)^2(1-b)^3} \mu_3 \end{aligned} \quad (55)$$

into (50) yields the following normal form with unfolding up to second order:

$$\dot{y}_1 = y_2 + O(|(y_1, y_2, \mu)|^3), \quad \dot{y}_2 = \beta_1(\mu) + \beta_2(\mu)y_2 - y_1^2 - \frac{2}{c}y_1y_2 + O(|(y_1, y_2, \mu)|^3).$$

Finally, introducing the transformation: $y_1 \rightarrow y_1, y_2 + O(|(y_1, y_2, \mu)|^3) \rightarrow y_2$ into the above system, we obtain

$$\dot{y}_1 = y_2, \quad \dot{y}_2 = \beta_1(\mu) + \beta_2(\mu)y_2 - y_1^2 - \frac{2}{c}y_1y_2 + O(|(y_1, y_2, \mu)|^3), \quad (56)$$

where

$$\begin{aligned} \beta_1(\mu) = & \frac{c^3(1+b)^2}{4b} \mu_1 - \frac{c^3(1+b)^2}{(1-b)^2} \mu_2 - \frac{(1-b)(1+b)^3c^2}{16b^3} \mu_3 - \frac{c^3(b+2)(1+b)}{4b(1-b)} \mu_1\mu_3 - \frac{c^3(1+b)}{b(1-b)^3} \mu_2\mu_3, \\ \beta_2(\mu) = & -\frac{(1-b^2)^2 + 48b^2c^2}{4b(1-b)^2} \mu_1 + \frac{(1-b^2)^2 + 32b^2c^2}{(1-b)^4} \mu_2 + \frac{(1+b)[(1-b^2)^2 + 16b^2c^2]}{16b^3c(1-b)} \mu_3 - \mu_4. \end{aligned} \quad (57)$$

Let

$$\det_{ij} = \det \left[\frac{\partial(\beta_1, \beta_2)}{\partial(\mu_i, \mu_j)} \right]_{\mu_1=\mu_2=0}.$$

Then, we have

$$\begin{aligned} \det_{12} &= -\frac{4bc^5(1+b)^2}{(1-b)^4}, & \det_{13} &= -\frac{c^4(1+b)^3}{2b^2(1-b)}, \\ \det_{14} &= -\frac{c^3(1+b)^2}{4b}, & \det_{23} &= \frac{c^4(1+b)^3}{b(1-b)^3}, \\ \det_{24} &= \frac{c^3(1+b)^2}{(1-b)^2}, & \det_{34} &= \frac{c^2(1-b)(1+b)^3}{16b^3}, \end{aligned} \tag{58}$$

showing that $\det_{ij} \neq 0$ for any of the six combinations. This shows that we can choose any two parameters from the six combinations such that system (56) with $(\beta_1, \beta_2) \approx (0, 0)$ for (x, y) near $(0, 0)$ is topologically equivalent to system (2) with $(\mu_i, \mu_j) \approx (0, 0)$ for (u, v) near $(u_3, v_3) = (\frac{1}{2}(1+b), \frac{1}{2}(1+b))$.

Since (56) is in the standard form of the BT bifurcation [Guckenheimer & Holmes, 1993; Kuznetsov, 1995], we apply the standard codimension-2 BT bifurcation theory to obtain the following result.

Theorem 8. For model (2), codimension-2 BT bifurcation occurs from the equilibrium $E_3 : (u, v) = (\frac{1}{2}(1+b), \frac{1}{2}(1+b))$ when $a = \frac{(1-b)^2 - 4bc}{4bc}$ and $m = \frac{(1-b)^2}{4b(1+a)}$ for $0 < b < 1$ and $c < \frac{(1-b)^2}{4b}$. Moreover, three local bifurcations with the representations of the bifurcation curves are given below.

- (1) Saddle-node bifurcation occurs from the bifurcation curve:

$$\text{SN} = \{(\beta_1, \beta_2) \mid \beta_1 = 0, \beta_2 > 0\}.$$

- (2) Hopf bifurcation occurs from the bifurcation curve:

$$\text{H} = \left\{ (\beta_1, \beta_2) \mid \beta_1 = \frac{c^2}{4}\beta_2^2, \beta_2 > 0, \text{subcritical} \right\}.$$

- (3) Homoclinic loop bifurcation occurs from the bifurcation curve:

$$\text{HL} = \left\{ (\beta_1, \beta_2) \mid \beta_1 = \frac{49}{25} \frac{c^2}{4}\beta_2^2, \beta_2 > 0, \text{unstable} \right\}.$$

The above formulas for bifurcation curves can be easily expressed in terms of the original perturbation parameters μ_1 and μ_2 by using (57). The

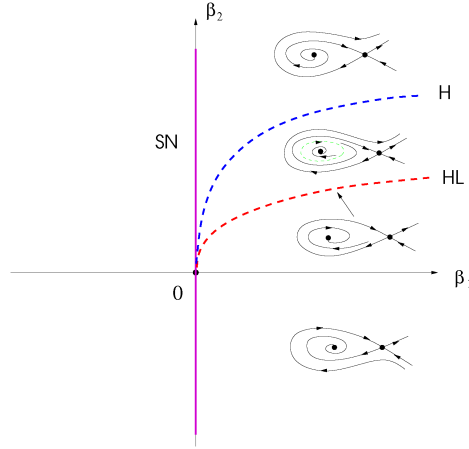


Fig. 6. Bifurcation diagrams for the codimension-2 BT bifurcation based on the normal form (56).

bifurcation diagram is depicted in Fig. 6. It can be seen from the item (2) in Theorem 8 that the Hopf bifurcation is subcritical, which agrees with Theorem 7

The numerical simulations for the BT bifurcation based on the original system (2) are shown in Figs. 2(c) and 4, where the values of parameters a and b are fixed, for which (47) becomes

$$\begin{aligned} m &= m^* = \frac{(1+a)(1-b)^2}{4b}, \\ c &= \frac{(1-b)^2}{4b(1+a)}, \quad (0 < b < 1). \end{aligned} \tag{59}$$

Then, the new formulas in (54)–(57) can be easily obtained by substituting the above solution of c into these equations. For the fixed values $a = b = \frac{1}{10}$, the equilibrium E_3 becomes $E_3 = (0.55, 0.55)$. The BT bifurcation critical point is given by $(m, c) = (m^*, c_u) = (\frac{891}{400}, \frac{81}{44}) = (2.2275, 1.840909\dots)$. For simplicity, we take $m = 2.2 < m^*$, and treat the parameter c as the bifurcation parameter. As shown in the bifurcation diagram given in Fig. 2(c), we choose 5 values of c near the BT bifurcation point along the vertical line $m = 2.2$: $c = 1.15, 1.35, 1.366035, 1.827766, 2.2$. It can be seen from this figure that for the point $(m, c) = (2.2, 1.15)$, E_{3+} is unstable, while E_{3+} is asymptotically stable at all other four points. Since Hopf bifurcation occurs at the point $(m, c) = (2.2, 1.218182)$, an unstable limit cycle bifurcates from the point $(m, c) = (2.2, 1.35)$, with the simulation depicted in Fig. 4(a). The unstable homoclinic loop appears at the point $(m, c) = (2.2, 1.366035)$,

with the simulation shown in Fig. 4(b). The heteroclinic orbits connecting the saddle E_1 and the saddle E_{3-} happen at the point $(m, c) = (2.2, 1.840909)$, as shown in Fig. 4(c), while that connecting the saddle E_1 and the stable focus E_{3+} occurs for $c > 1.840909$ ($m = 2.2$), with the simulated example shown in Fig. 4(d) by taking $m = c = 2.2$.

6. Numerical Simulations

In this section, we present numerical simulations to illustrate the analytical results obtained in the previous sections. The simulation results are obtained using the numerical bifurcation package MATCONT [Dhooge et al., 2003] with the fixed values $a = b = \frac{1}{10}$. First, we present a numerical bifurcation diagram of system (2) on the two-dimensional m - c parameter plane, as shown in Fig. 7 where SN, H, BT and HL denote the saddle-node, Hopf, BT and homoclinic bifurcations, respectively. This bifurcation diagram is similar to that shown in Fig. 2(c), but here, the homoclinic loop bifurcation curve is numerically obtained. The three bifurcation curves (SN, H and HL) divide the parameter plane into four regions with different colors: red for region I, blue for region II, black for region III and green for region IV.

Note that system (2) always has the asymptotically stable trivial equilibrium E_0 and two unstable

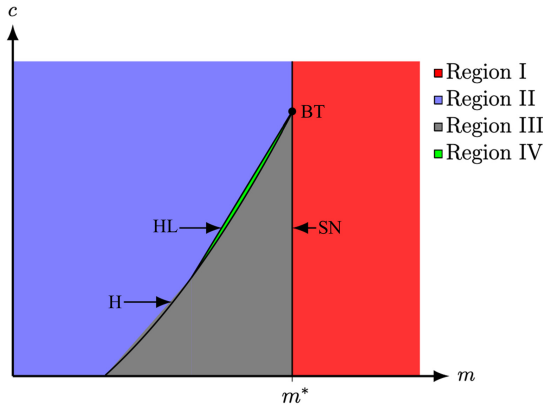


Fig. 7. Bifurcation diagram of system (2), obtained using MATCONT, plotted on the m - c parameter plane for $a = b = \frac{1}{10}$, where SN, H, BT and HL represent the saddle-node, Hopf, BT and homoclinic bifurcations, respectively. The system undergoes a saddle-node bifurcation from E_3 at $m = m^*$ ($c \neq c_u$), and a codimension-2 BT bifurcation occurs from E_3 at $(m, c) = (m^*, c_u)$. For $m < m^*$, Hopf bifurcation occurs from E_{3+} , and homoclinic loop bifurcation curve is determined by the BT bifurcation.

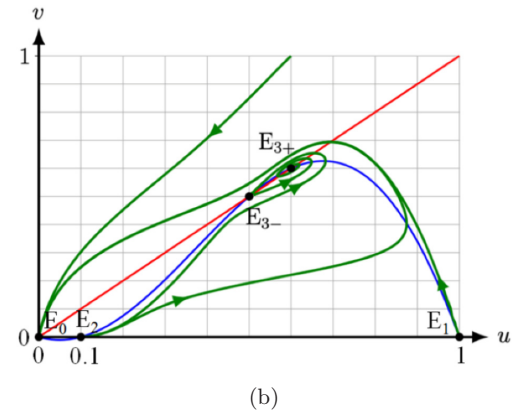
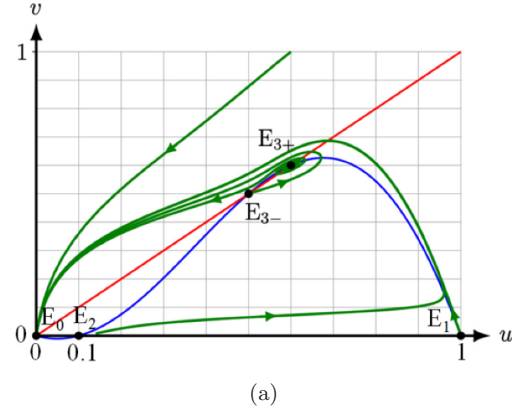


Fig. 8. Simulated phase portraits of system (2), obtained using MATCONT, for $a = b = 0.1, m = 2.2$: (a) when $c = 1.2$ showing the saddle point E_1 , unstable node E_2 , saddle point E_{3-} and unstable focus E_{3+} ; and (b) when $c = 1.5$ showing the saddle point E_1 , unstable node E_2 , saddle point E_{3-} and stable focus E_{3+} ; The stable manifold of E_{3-} connects E_2 to form the heteroclinic orbit $\Gamma_{E_2 E_{3-}}$.

boundary equilibria E_1 and E_2 . The bifurcation diagram given in Fig. 7 shows different bifurcations from the positive equilibria. In the region I (red color), there do not exist positive equilibria. When the parameter m is varied to cross the boundary line $m = m^*$ ($c \neq c_u$), the saddle-node bifurcation occurs from the equilibrium E_3 , yielding two positive equilibria $E_{3\pm}$ in the regions II, III and IV, and the equilibrium E_{3-} is always unstable (a saddle point). The BT bifurcation appears at the critical point $(m, c) = (m^*, c_u)$ at which the regions I, II and III intersect at one point. The positive equilibrium E_{3+} is asymptotically stable in the region II (blue color), and loses its stability on the Hopf critical curve, and becomes unstable in the region III (black color). The homoclinic loop (HL) bifurcation occurs near the BT bifurcation point, and the small

green region IV corresponds to the area between the H and HL curves in the BT bifurcation diagram in Fig. 6, where an unstable limit cycle exists. It should be pointed that in general the unstable limit cycle bifurcates from any critical point on the H curve.

According to different bifurcation results given in Theorems 2, 7 and 8, various parameter values are chosen to illustrate different bifurcation phenomena. Besides the simulations shown in Figs. 4 and 5, we choose two more sets of parameter values to give the simulations as depicted in Fig. 8, where the red and blue curves represent the predator and nullclines, respectively. For Figs. 4 and 8, we choose $a = b = 0.1$, $m = 2.2$ and vary c , while for Fig. 5(a), we also change m from $m = 2.2$ to $m = 2.2275$. Only Fig. 4(a) shows bifurcation of an unstable limit cycle, while other figures demonstrate different dynamical behaviors of system (2). Figure 5 shows a single positive equilibrium E_3 which is a cusp point, while all other figures show two positive equilibria $E_{3\pm}$. Figure 8(a) shows that all equilibria, except E_0 , are unstable, while Fig. 8(b) depicts a heteroclinic curve, connecting E_2 and E_{3-} . It is seen from this figure that when the initial value of the prey with strong Allee effect is smaller than that of the predator, the solution trajectories converge to $(0, 0)$, which implies that both predator and prey will become extinct. On the contrary, when the initial value of the prey with strong Allee effect is bigger than that of the predator, the solution trajectories converge to $(0, 0)$ or E_{3+} , implying that both predator and prey will become extinct or coexist.

7. Conclusion

In this paper, we have investigated the bifurcation and dynamics of a Leslie–Gower predator–prey system with strong Allee effect in prey and ratio-dependent functional response. The positivity of the solutions and their boundedness are established. The system can have at most five equilibria. The trivial solution $E_0 = (0, 0)$ is a degenerate singular point, and is proved asymptotically stable by using the blow-up approach. Moreover, a number of results relative to the global dynamics of the system connected to the property of the origin are established. Two unstable boundary equilibria always exist, but positive equilibria may exist under certain parameter conditions. Various bifurcations can occur, including the saddle-node, Hopf and BT bifurcations. It is proved that the Hopf bifurcation has codimension-1, implying that no multiple limit

cycle bifurcation can happen. The codimension-2 BT bifurcation occurs only for certain set of parameters. Finally, numerical simulations are presented to illustrate the theoretical results.

Various bifurcations obtained in this paper for the predator–prey model with strong Allee effect and ratio-dependent functional reveal that the Allee effect greatly influences the dynamical behaviors of the system. In particular, it has been shown the system gets more chance for both the predator and prey to become extinct when the density level of the prey is below the critical threshold $u = b$. When positive (coexisting) equilibria exist, the system may exhibit bistable phenomenon, that is, both E_0 and E_3 , or E_0 and E_{3-} are stable. For the latter case, an unstable limit cycle arises from Hopf bifurcation, implying the predator and prey in a oscillating phase. Our findings indicate that even when the system exists in the oscillating model, the system still has great possibility for both predator and prey to become extinct due to the impact of the Allee effect.

The methodology discussed in this paper is a complement to the existing approaches, and may be applied to study complex dynamics and bifurcations for other biological and physical systems.


Acknowledgment

This work was partially supported by the National Natural Science Foundation of China, No. U1604180 (J. F. Zhang) and the Natural Sciences and Engineering Research Council of Canada, No. R2686A2 (P. Yu).

ORCID

Pei Yu 

<https://orcid.org/0000-0002-8848-0584>

Jia-Fang Zhang 

<https://orcid.org/0000-0001-5767-1786>

Claudio Arancibia-Ibarra 

<https://orcid.org/0000-0001-9725-7029>

References

- Allee, W. C. & Aggregations, A. [1931] *A Study in General Sociology* (University of Chicago Press, Chicago).
- Arancibia-Ibarra, C., Flores, J., Pettiet, G. & Van Heijster, P. [2019] “A Holling–Tanner predator–prey model with strong Allee effect,” *Int. J. Bifurcation and Chaos* **29**, 1930032-1–16.

- Arancibia-Ibarra, C. & Flores J. [2021] “Dynamics of a Leslie–Gower predator–prey model with Holling type II functional response, Allee effect and a generalist predator,” *Math. Comput. Simul.* **188**, 1–22.
- Arino, O., Mikram, J. & Chattopadhyay, J. [2004] “Infection on prey population may act as a biological control in ratio-dependent predator–prey model,” *Nonlinearity* **17**, 1101–1116.
- Artidi, R. & Ginzburg, L. R. [1989] “Coupling in predator–prey dynamics: Ratio-dependence,” *J. Theor. Biol.* **139**, 311–326.
- Bazykin, A. D. [1998] *Nonlinear Dynamics of Interacting Populations* (World Scientific, Singapore).
- Beretta, E. & Kuang, Y. [1998] “Global analyses in some delayed ratio-dependent predator–prey systems,” *Nonlinear Anal.* **32**, 381–408.
- Berryman, A. A. [1992] “The origins and evolution of predator–prey theory,” *Ecology* **73**, 1530–1535.
- Boukal, D. S., Sabelis, M. W. & Berec, L. [2007] “How predator functional responses and Allee effects in prey affect the paradox of enrichment and population collapses,” *Theor. Popul. Biol.* **72**, 136–147.
- Dhooge, A., Govaerts, W. & Kuznetsov, Y. A. [2003] “MATCONT: A MATLAB package for numerical bifurcation analysis of ODEs,” *ACM Trans. Math. Softw.* **29**, 141–164.
- Freedman, H. I. [1980] *Deterministic Mathematical Models in Population Ecology* (Marcel Dekker, NY).
- Gascoigne, J. & Lipcius, R. [2004] “Allee effects driven by predation,” *J. Appl. Ecol.* **41**, 801–810.
- Guckenheimer, J. & Holmes, P. [1993] *Nonlinear Oscillations, Dynamical Systems, and Bifurcations of Vector Fields*, 4th edition (Springer, NY).
- Holling, C. S. [1965] “The functional response of predator to prey density and its role in mimicry and population regulation,” *Men. Ent. Sec. Can.* **91**, 385–398.
- Hsu, S. B., Hwang, T. W. & Kuang, Y. [2001a] “Rich dynamics of ratio-dependent one prey two predators model,” *J. Math. Biol.* **43**, 377–396.
- Hsu, S. B., Hwang, T. W. & Kuang, Y. [2001b] “Global analysis of the Michaelis–Menten-type ratio-dependent predator–prey system,” *J. Math. Biol.* **42**, 489–506.
- Huo, H. F. & Li, W. T. [2004] “Stable periodic solution of the discrete periodic Leslie–Gower predator–prey model,” *Math. Comput. Model.* **40**, 261–269.
- Korobeinikov, A. [2001] “A Lyapunov function for Leslie–Gower predator–prey models,” *Appl. Math. Lett.* **14**, 697–699.
- Kuang, Y. & Beretta, E. [1998] “Global qualitative analysis of a ratio-dependent predator–prey system,” *J. Math. Biol.* **36**, 389–406.
- Kuznetsov, Y. A. [1995] *Elements of Applied Bifurcation Theory* (Springer-Verlag, NY).
- Lajmiri, Z. Ghaziani, R. K. & Orak, I. [2018] “Bifurcation and stability analysis of a ratio-dependent predator–prey model with predator harvesting rate,” *Chaos Solit. Fract.* **106**, 193–200.
- Leslie, P. H. & Gower, J. C. [1960] “The properties of a stochastic model for the predator–prey type of interaction between two species,” *Biometrika* **47**, 219–234.
- Lewis, M. A. & Kareiva, P. [1993] “Allee dynamics and the spread of invading organisms,” *Theor. Popul. Biol.* **43**, 141–158.
- Lotka, A. J. [1925] *Elements of Physical Biology* (Williams and Wilkins, Baltimore).
- Lu, M., Huang, J., Ruan, S. & Yu, P. [2021] “Global dynamics of a susceptible-infectious-recovered epidemic model with a generalized nonmonotone incidence rate,” *J. Dyn. Differ. Equ.* **33**, 1625–1661.
- Mainul, H. [2009] “Ratio-dependent predator–prey models of interacting populations,” *Bull. Math. Biol.* **71**, 430–452.
- May, R. M. [2001] *Stability and Complexity in Model Ecosystems* (Princeton University Press, NJ).
- Morozov, A. Petrovskii, S. & Li, B. L. [2006] “Spatiotemporal complexity of patchy invasion in a predator–prey system with the Allee effect,” *J. Theor. Biol.* **238**, 18–35.
- Ni, W. & Wang, M. X. [2017] “Dynamical properties of a Leslie–Gower prey–predator model with strong Allee effect in prey,” *Discrete Contin. Dyn. Syst. Ser. B* **22**, 3409–3420.
- Pal, P. J. & Mandal, P. K. [2014] “Bifurcation analysis of a modified Leslie–Gower predator–prey model with Beddington–DeAngelis functional response and strong Allee effect,” *Math. Comput. Simul.* **97**, 123–146.
- Pielou, E. C. [1969] *An Introduction to Mathematical Ecology* (Wiley Interscience, John Wiley and Sons, NY).
- Ruan, S. & Xiao, D. [2000] “Global analysis in a predator–prey system with nonmonotonic functional response,” *SIAM J. Appl. Math.* **61**, 1445–1472.
- Sen, D., Ghorai, S., Banerjee, M. & Morozov, A. [2022] “Bifurcation analysis of the predator–prey model with the Allee effect in the predator,” *J. Math. Biol.* **84**, 1–27.
- Song, Y. L., Yuan, S. L. & Zhang, J. M. [2009] “Bifurcation analysis in the delayed Leslie–Gower predator–prey system,” *Appl. Math. Model.* **33**, 4049–4061.
- Verma, M. & Misra, A. K. [2018] “Modeling the effect of prey refuge on a ratio-dependent predator–prey system with the Allee effect,” *Bull. Math. Biol.* **80**, 626–656.
- Volterra, V. [1926] “Fluctuations in the abundance of a species considered mathematically,” *Nature* **118**, 558–560.

- Wang, M. H. & Kot, M. [2002] “Speeds of invasion in a model with strong or weak Allee effects,” *Math. Biosci.* **171**, 83–97.
- Wang, J., Shi, J. & Wei, J. [2003] “Predator–prey system with strong Allee effect in prey,” *J. Math. Biol.* **62**, 291–331.
- Xiao, D. & Ruan, S. [2001] “Global dynamics of a ratio-dependent predator–prey system,” *J. Math. Biol.* **43**, 268–290.
- Yan, X. P. & Li, W. T. [2006] “Hopf bifurcation and global periodic solutions in a delayed predator–prey system,” *Appl. Math. Comput.* **177**, 427–445.
- Yu, P. [1998] “Computation of normal forms via a perturbation technique,” *J. Sound Vib.* **211**, 19–38.
- Yu, P. & Bi, Q. [1998] “Analysis of non-linear dynamics and bifurcations of a double pendulum,” *J. Sound Vib.* **217**, 691–736.
- Zeng, B., Deng, S. F. & Yu, P. [2020] “Bogdanov–Takens bifurcation in predator–prey systems,” *Discrete Contin. Dyn. Syst., Ser. S* **13**, 3253–3269.
- Zeng, Y. & Yu, P. [2022] “Complex dynamics of predator–prey systems with Allee effect,” *Int. J. Bifurcation and Chaos* **32**, 2250203–1–35.
- Zhang, Z., Ding, T., Huang, W. & Dong, Z. [1991] *Qualitative Theory of Differential Equations*, Translations of Mathematical Monographs 101 (American Mathematical Society, Providence).
- Zhang, J. F., Lou, W. P. & Wang, Y. X. [2022] “The role of strong Allee effect and protection zone on a diffusive prey–predator model,” *Z. Angew. Math. Phys.* **73**, 1–23.